PL-TR-94-2235

TWO-DIMENSIONAL SIGNAL PROCESSING FOR REGIONAL SEISMIC EVENT IDENTIFICATION

Jay J. Pulli
Paul S. Dysart

Radix Systems, Inc.
6 Taft Court
Rockville, MD 20850

September 1994

Final Report
3 June 1993 - 31 August 1994

PHILLIPS LABORATORY
Directorate of Geophysics
AIR FORCE MATERIEL COMMAND
HANSCOM AIR FORCE BASE, MA 01731-3010

SPONSORED BY
Advanced Research Projects Agency (DoD)
Nuclear Monitoring Research Office
ARPA ORDER NO 128

MONITORED BY
Phillips Laboratory
CONTRACT NO. F19628-93-C-0060

This technical report has been reviewed and is approved for publication.

JAMES F. LEWKOWICZ
Contract Manager
Earth Sciences Division

JAMES F. LEWKOWICZ, Director
Earth Sciences Division

This report has been reviewed by the ESC Public Affairs Office (PA) and is releasable to the National Technical Information Service (NTIS).

Qualified requestors may obtain additional copies from the Defense Technical Information Center. All others should apply to the National Technical Information Service.

If your address has changed, or if you wish to be removed from the mailing list, or if the addressee is no longer employed by your organization, please notify PL/TSI, 29 Randolph Road, Hanscom AFB, MA 01731-3010. This will assist us in maintaining a current mailing list.

Do not return copies of this report unless contractual obligations or notices on a specific document requires that it be returned.

REPORT DOCUMENTATION PAGE

Form Approved
OMB No. 0704-0188

1. AGENCY USE ONLY (Leave blank)	2. REPORT DATE	3. REPORT TYPE AND DATES COVERED
	September 1994	Final (3 Jun 1993-31 August 1994)

4. TITLE AND SUBTITLE
Two-Dimensional Signal Processing for Regional Seismic Event Identification

5. FUNDING NUMBERS
PE 62301E
PR NM93 TA GM WU AH

Contract F19628-93-C-0060

6. AUTHOR(S)
Jay J. Pulli
Paul S. Dysart

7. PERFORMING ORGANIZATION NAME(S) AND ADDRESS(ES)
Radix Systems, Inc.
6 Taft Court
Rockville, MD 20850

8. PERFORMING ORGANIZATION REPORT NUMBER

9. SPONSORING/MONITORING AGENCY NAME(S) AND ADDRESS(ES)
Phillips Laboratory
29 Randolph Road
Hanscom AFB, MA 01731-3010

Contract Manager: James Lewkowicz/GPEH

10. SPONSORING/MONITORING AGENCY REPORT NUMBER
PL-TR-94-2235

11. SUPPLEMENTARY NOTES

12a. DISTRIBUTION/AVAILABILITY STATEMENT
Approved for public release;
distribution unlimited

12b. DISTRIBUTION CODE

13. ABSTRACT *(Maximum 200 words)*

The objective of this research was to develop a methodology for regional seismic event identification which utilizes 2-dimensional signal processing and treats the seismogram as an image. The motivation for this research comes from the observation that the spectral features which distinguish quarry explosions from earthquakes can be seen throughout the entire seismogram. These features, which include spectral banding, are apparent in the time-frequency (TF) representation of the seismogram.

We parameterized the TF representation by computing the wavenumber spectrum of the image and fitting this to a stochastic surface model developed to characterize bathymetric surfaces. Five model parameters control image features such as lineations, spatial orientation, characteristic lengths, and roughness of the surface. In addition, 19 other features were extracted using image processing techniques (e.g. eigenvalues and curtosis). These 24 parameters were extracted from ground truth databases of seismic events covering NORESS, Vogtland, and Lubin. The parameters were evaluated in terms of their ability to separate seismic event source types using the Mahalanobis Distance. In general, 5 of the 24 image parameters provide the best ability to separate source types. The study shows that image parameters derived from the entire seismogram provide additional useful information (i.e. in addition to parameters such as the Lg/P spectral ratio) for source type identification.

14. SUBJECT TERMS	15. NUMBER OF PAGES
Seismic Explosion Earthquake Identification Image Processing	50
	16. PRICE CODE

17. SECURITY CLASSIFICATION OF REPORT	18. SECURITY CLASSIFICATION OF THIS PAGE	19. SECURITY CLASSIFICATION OF ABSTRACT	20. LIMITATION OF ABSTRACT
Unclassified	Unclassified	Unclassified	SAR

Table of Contents

List of Figures

List of Tables

1. Introduction

The objective of this research effort is to develop and test a methodology for regional seismic event identification which utilizes 2-dimensional signal processing and treats the seismogram as an *image*. The methodology seeks to exploit the information content of an entire regional seismogram, and is particularly appropriate for small events, multiple events, and events with blocked, attenuated, or missing phases.

The motivation for this research comes from our observation that the spectral features which distinguish quarry explosions from naturally occurring earthquakes can be seen throughout the entire seismogram. These features, which include the spectral complexity and spectral energy distribution (*P vs. S*), are readily apparent in the time-frequency (TF) representation of the seismogram[1]. The TF distribution is particularly helpful in the analysis of events which have highly attenuated, blocked, or missing phases.

A number of investigators have pointed out the utility of the TF distribution for seismic analysis (Smith, 1989; Hedlin *et al.*, 1989). However, TF plots have not been widely used or accepted in the seismic community. There are a number of reasons for this situation: the difficulty of manipulating and operating on 2-D images *vs.* 1-D time series or spectra; the lack of quantifiable measures of the features seen on TF plots; the lack of simple relations between TF images and the physics of the source and propagation effects; and the lack of a simple image discriminator which would allow automated processing of TF images.

During the course of our research on the application of artificial neural networks (ANN's) to seismic event identification, we have employed TF plots for

---

[1] The time-frequency distribution goes by many names. Examples include *spectrogram* and *sonogram*. We prefer the general term *time-frequency distribution*, because it includes many different types of distributions, such as Wigner-Ville, and special window functions such as the cone kernel. A spectrogram or sonogram implies a specific type of distribution.

the purposes of data review and phase timing. This use has led us to be able to perform simple visual classification of TF images which closely match the classification capability of our 1-D ANN-based processor. However, the TF image appears to excel in situations of low SNR, mixed events, or events with highly attenuated phases. Preliminary research has shown that we can exploit the information content of a TF distribution by first transforming the TF image into the wavenumber domain via a 2-D FFT, and then use a combination of image processing and simple backpropagation ANN's to extract a number of features which completely describe the spatio-temporal nature of the source. These features can then be input to any number of classifiers to perform the final event identification.

This report documents our study to test the utility of these concepts for regional seismic event identification. The study focuses on events from the NORESS, Vogtland, and Lubin ground truth databases used in our previous studies of regional discrimination (Pulli and Dysart, 1993).

2. Signal Processing and Parameter Extraction

2.1 Step 1: Time-Frequency Transformation

Step 1 of our analysis involves the transformation of the original time series data (single station or array) into the time-frequency (TF) domain. There are numerous schemes for implementing the TF transformation (Cohen, 1989), the simplest of which is to slide a tapered window down the time series and compute successive FFT's. The result can be displayed in a number of ways, but we prefer a 2-dimensional color-coded representation for simplicity. *Figure 1* shows the TF images of two demonstration events recorded at the NORESS array. The event at the top is a quarry blast at the Titania Mine, southwest of NORESS. Note the spectral banding seen throughout the TF image. The event at the bottom is a nearby earthquake. No spectral banding is present in its TF image. The TF image of the earthquake is dominated by energy around the *Lg* wave.

2.2 Step 2: Image Equalization

Image equalization refers to the process by which the images are enhanced, corrected, or detrended to bring out specific features of the image. An analogy in 1-dimensional seismic signal processing would be the correction of seismic spectra for f^{-2} spectral decay or attenuation. Three different image equalization schemes were applied to the TF distributions.

Equalization 1 treats the TF image as a sequence of power time-series (essentially narrow bandpass filtered seismograms, one frequency at a time) and applies noise-spectral equalization to the rows (time series) of the image. This equalization emphasizes the relative energy in each frequency bin as a function of time, and tends to enhance the *Pn/Lg* spectral ratio information in the whole

seismogram. It also enhances the spectral banding seen in the ripple-fired quarry blasts (Smith, 1989; Hedlin *et al.*, 1989).

Equalization 2 treats the TF image as a sequence of power spectra and applies noise-spectral equalization to the columns (spectra) of the image to obtain deviations from the trend of the power spectra. This equalization emphasizes the spectral banding seen in the ripple-fired quarry blasts and de-emphasizes the *Pn/Lg* spectral ratio information.

Equalization 3 is similar to equalization 1 in that it operates on the rows (time-series) of the TF distribution, but it this case it determines deviations in the trends of the time series. This effectively removes the seismic phase amplitude ratio information and the frequency banding, leaving whatever is left to dominate. Hence, this equalization is a residual estimate of the TF iamge.

2.3 Step 3: Wavenumber Transformation

In Step 3, the TF image is transformed into the wavenumber domain using a 2-D FFT. The wavenumber representation of the demonstration events is shown in *Figure* 2. A variety of options exist at this stage, including the use of alternative 2-D images such as cepstra vs. time, *Lg/Pn* spectral ratios vs. time, binary images, and higher dimensional images.

2.4 Step 4: Image Model and Image Parameters

A key element of our methodology is the use of a parametric model to characterize the power spectrum of an arbitrary image. The model we have used is a stochastic surface model originally developed by Goff and Jordan (1989) to characterize bathymetric surfaces. The power spectral form of the model is given by

$$P(k) = \frac{4\pi v H^2}{\sqrt{|Q|}}\left[u^2(k)+1\right]^{-(v+1)} \tag{1}$$

where H is the RMS height (energy), k is the wavenumber, Q is a matrix given by

$$Q = \begin{bmatrix} k_s^2\sin^2(\theta)+k_n^2\cos^2(\theta) & \left(k_n^2-k_s^2\right)\sin^2(\theta)\cos^2(\theta) \\ \left(k_s^2-k_n^2\right)\sin^2(\theta)\cos^2(\theta) & k_n^2\sin^2(\theta)+k_s^2\cos^2(\theta) \end{bmatrix} \tag{2}$$

and θ is the azimuth. The exponential term ν is related to a constant asymptotic slope (B) of the power spectrum, or fractal dimension (D), each of which implies a surface whose amplitudes scale predictably with wavenumber. B and D are related to ν by

$$B = -2(v+1)$$
$$D = 3 - v \tag{3}$$

These parameters quantify features such as lineations, spatial orientation, characteristic lengths, and roughness.

In summary, the model of the wavenumber image is characterized by 5 features:

- H: the RMS height, or energy of the wavenumber spectrum
- θ: the azimuth of symmetry
- k_S: the characteristic wavenumber parallel to the axis of symmetry
- k_n: the characteristic wavenumber normal to the axis of symmetry
- B: the asymptotic slope

In addition to these 5 model parameters, we extracted an additional 19 image parameters using techniques from image processing (such as the Karhunen-Loeve transform). This transform determines the covariance structure and higher-order moments of the image by assuming that the image represents a pseudo-probability density function. The covariance of the zero-mean image is

$$COV[P(kx,ky)] = \begin{Bmatrix} S_{11} & S_{12} \\ S_{21} & S_{22} \end{Bmatrix} \tag{4}$$

where

$$S_{11} = \sum_{i=1}^{n} \frac{(kx_i - \bar{k}x)^2}{n-1} \sum_{j=1}^{n} P(kx,ky) \tag{5}$$

$$S_{22} = \sum_{j=1}^{n} \frac{(ky_i - \bar{k}y)^2}{n-1} \sum_{i=1}^{n} P(kx,ky)$$

$$S_{12} = \sum_{i=1}^{n} \sum_{j=1}^{n} \frac{(kx_i - \bar{k}x)(ky_j - \bar{k}y)}{n-1} P(kx,ky)$$

The eigenvalue problem is solved by the singular value decomposition (SVD) of the covariance matrix

$$SVD(COV) = U \begin{Bmatrix} e_1^2 & 0 \\ 0 & e_2^2 \end{Bmatrix} V^T \tag{6}$$

Although not required in the 2X2 case, the SVD method is included by our analysis to allow parameter extraction from higher-dimensional images.

The parameters determined by this analysis, as well as their names as used in subsequent plots, are shown in the following table.

Table 1. List of parameters extracted from wavenumber images.

Parameter	Definition	Parameter Name on Plots
e_{11}	1st Eigenvalue, i=1	emajor
e_{12}	1st Eigenvalue, i=2	emajor-2
e_{13}	1st Eigenvalue, i=3	emajor-3
e_{21}	2nd Eigenvalue, i=1	eminor
e_{22}	2nd Eigenvalue, i=2	eminor-2
e_{23}	2nd Eigenvalue, i=3	eminor-3
$kurt_1$	Image kurtosis, i=1	curt
$kurt_2$	Image kurtosis, i=2	curt-2
$kurt_3$	Image kurtosis, i=3	curt-3
e_{11}/e_{21}	Eigenvalue ratio, i=1	emajor/eminor
e_{12}/e_{22}	Eigenvalue ratio, i=2	emajor-2/eminor-2
e_{13}/e_{23}	Eigenvalue ratio, i=3	emajor-3/eminor-3
$e_{11} \times e_{21}$	Eigenvalue product, i=1	emajor x eminor
$e_{12} \times e_{22}$	Eigenvalue product, i=2	emajor-2 x eminor-2
$e_{13} \times e_{23}$	Eigenvalue product, i=3	emajor-3 x eminor-3
$\sqrt{e_{11}^2 + e_{21}^2}$	Eigenvalue norm, i=1	eigen_norm
$\sqrt{e_{12}^2 + e_{22}^2}$	Eigenvalue norm, i=1	eigen2_norm
$\sqrt{e_{13}^2 + e_{23}^2}$	Eigenvalue norm, i=1	eigen3_norm
e_{13}/e_{22}	Eigenvalue ratio, i=3, j=2	emajor-3/emajor-2
Kurt3 / Kurt2	Kurtosis ratio	curt-3/curt-2
k_s	Characteristic length	1/ws
k_n	Characteristic length	1/wn
H	RMS height	rms
B	Spectral slope	hexp

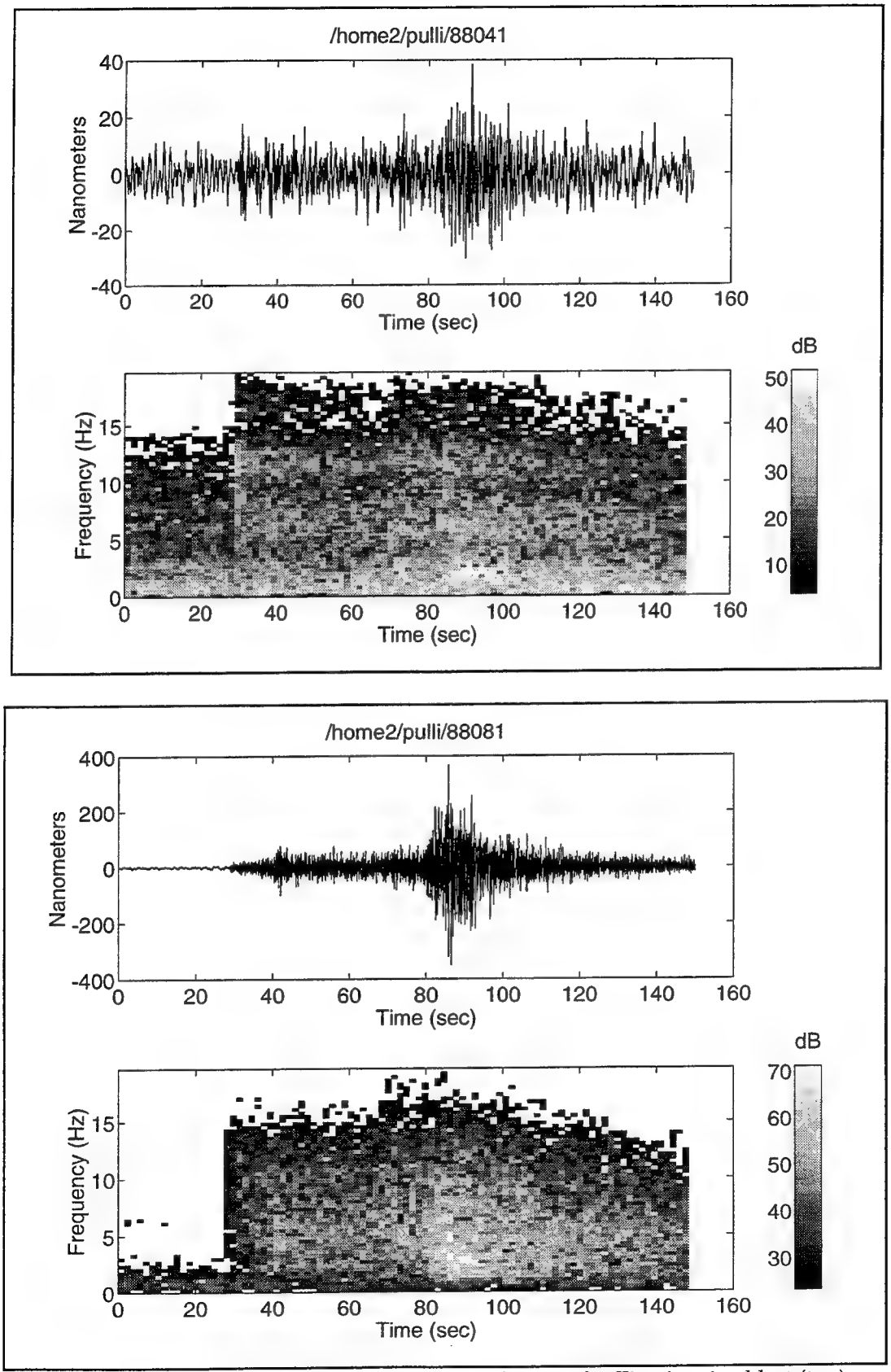

Figure 1. Time series and time-frequency distributions for Titania mine blast (top) and coastal Norway earthquake (bottom).

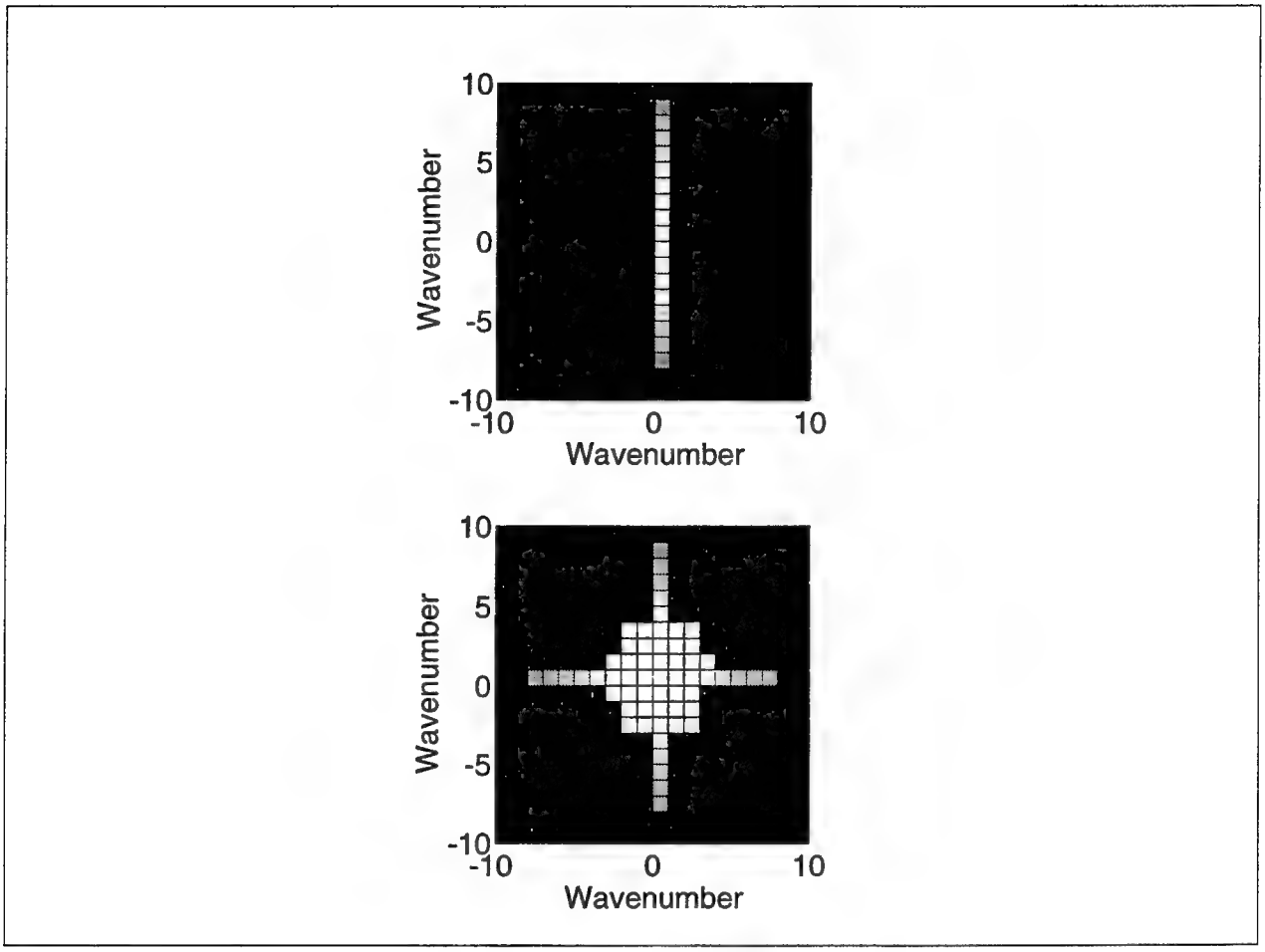

Figure 2. Wavenumber spectra of Titania mine blast (top) and coastal earthquake (bottom).

3. Results for NORESS, Vogtland, and Lubin

3.1 NORESS

The methodology just described was first applied to 83 events from our NORESS ground truth database described in previous documents (e.g. Pulli and Dysart, 1994). Of these 83 events, 35 were earthquakes and 48 were explosions. The 24 image parameters were extracted for all of the events using each of the three image equalization schemes. Values of these parameters are shown graphically in *Figures 3-8.*

It is clear from these plots that some of the image parameters are quite good at separating event types, such as curtosis for equalizations 1 and 2. However, many parameters provide little or no capability for separating event classes. An effective means of condensing and evaluating these parameters is the calculation of the Mahalanobis Distance, which is

$$D_p = \frac{(\mu_1 - \mu_2)^2}{\sigma_1^2 + \sigma_2^2} \qquad (7)$$

Here, μ and σ are the means and variances respectively of the parameter values for each class of events (1 and 2). Parameters which provide good identification capability have large differences in mean values and small variances, and hence large D_p's. The best parameters from equalization 1 are:

- 20: eminor 3
- 1: curtosis
- 10: emajor-2 / eminor-2
- 18: eminor

For equalization 2, the best parameters are:

- 2: curtosis 2
- 1: curtosis
- 4: curtosis-3 / curtosis-2
- 22: rms
- 19: eminor 2

For equalization 3, the best parameters are:

- 15: emajor-3 x eminor-3
- 19: eminor 2
- 4: curtosis-3 / curtosis-2
- 22: rms
- 2: curtosis-2

3.2 Vogtland

The Vogtland dataset (see Grant *et al.*, 1994; Pulli and Dysart, 1994) consists of 23 events, 9 earthquakes and 14 explosions. Parameter values for the three image equalization schemes are shown in *Figures 12-17*. Mahalanobis Distances are plotted in *Figures 18-20*. The best parameters from equalization 1 are:

- 18: eminor
- 20: eminor-3
- 1: curtosis

- 15: emajor -3 x eminor-3
- 4: curtosis-3 / curtosis-2
- 22: rms

For equalization 2, the best parameters are:

- 18: eminor
- 1: curtosis
- 23: wn
- 24: ws
- 21: hexp

For equalization 3, the best parameters are:

- 9: emajor 2
- 5: eigen2_norm
- 13: emajor-3 / emajor-2
- 11: emajor-2 x eminor-2

3.3 Lubin

The Lubin dataset consists of 30 "mining-induced earthquakes". Image parameters for the three equalizations are shown in *Figures 21-26*. Since there is only one source type in this dataset, Mahalahobis Distance calculations are not appropriate, but a comparison of the image parameters with those of the nearby Vogtland events is of interest. We will take the best parameters from equalization and note under which class the Lubin events fall.

The best parameters from equalization 1 are:

- 18: eminor - Lubin events fall primarily under explosion class
- 20: eminor-3 - Lubin events fall under both classes
- 1: curtosis - Lubin events fall under earthquake class
- 15: emajor-3 x eminor-3 - Lubin events fall primarily under explosion class
- 4: curtosis-3 / curtosis-2 - Lubin events fall primarily under explosion class
- 22: rms - Lubin events fall under earthquake class

For equalization 2, the best parameters are:

- 18: eminor - Lubin events fall primarily under explosion class
- 1: curtosis - Lubin events fall primarily under explosion class
- 23: wn - Lubin events fall primarily under explosion class
- 24: ws - Lubin events fall primarily under explosion class
- 21: hexp - Lubin events fall primarily under explosion class

For equalization 3, the best parameters are:

- 9: emajor 2 - Lubin events fall under both classes
- 5: eigen2_norm - Lubin events fall primarily under explosion class
- 13: emajor-3 / emajor-2 - Lubin events fall under both classes
- 11: emajor-2 x eminor-2 - Lubin events fall primarily under explosion class

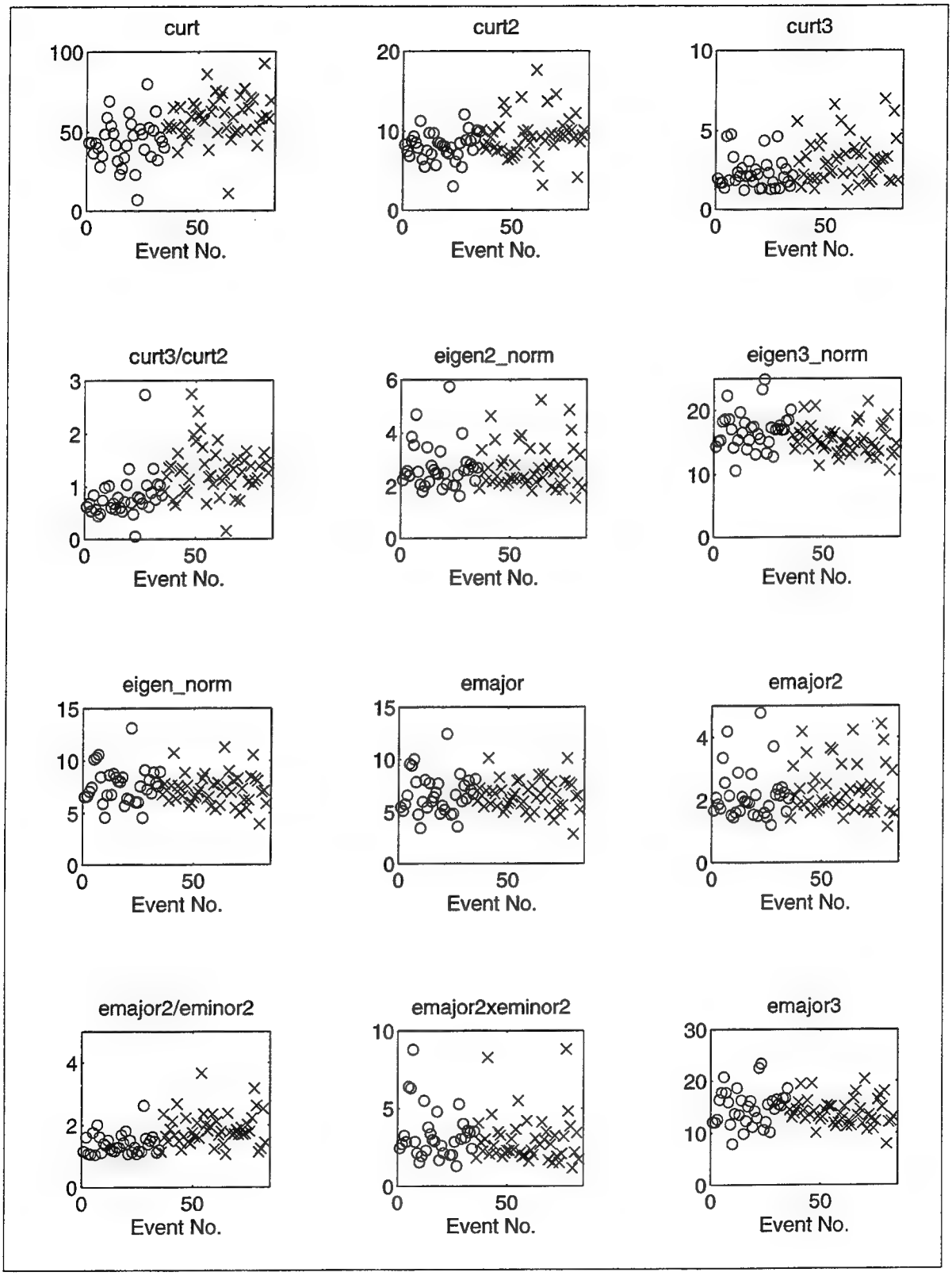

Figure 3. Values of image parameters 1-12 for the NORESS dataset, equalization number 1.

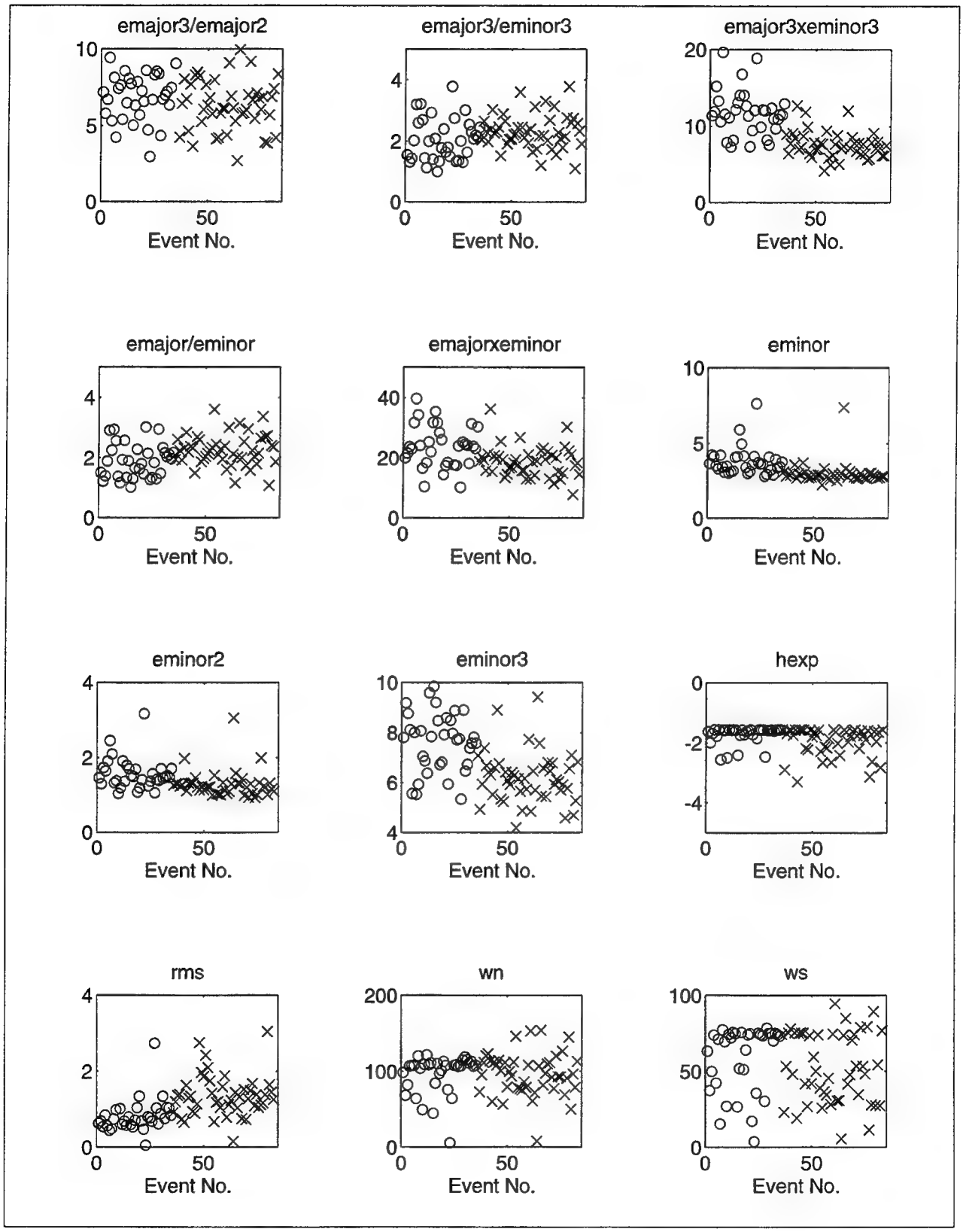

Figure 4. Values of image parameters 13-24 for the NORESS dataset, equalization number 1.

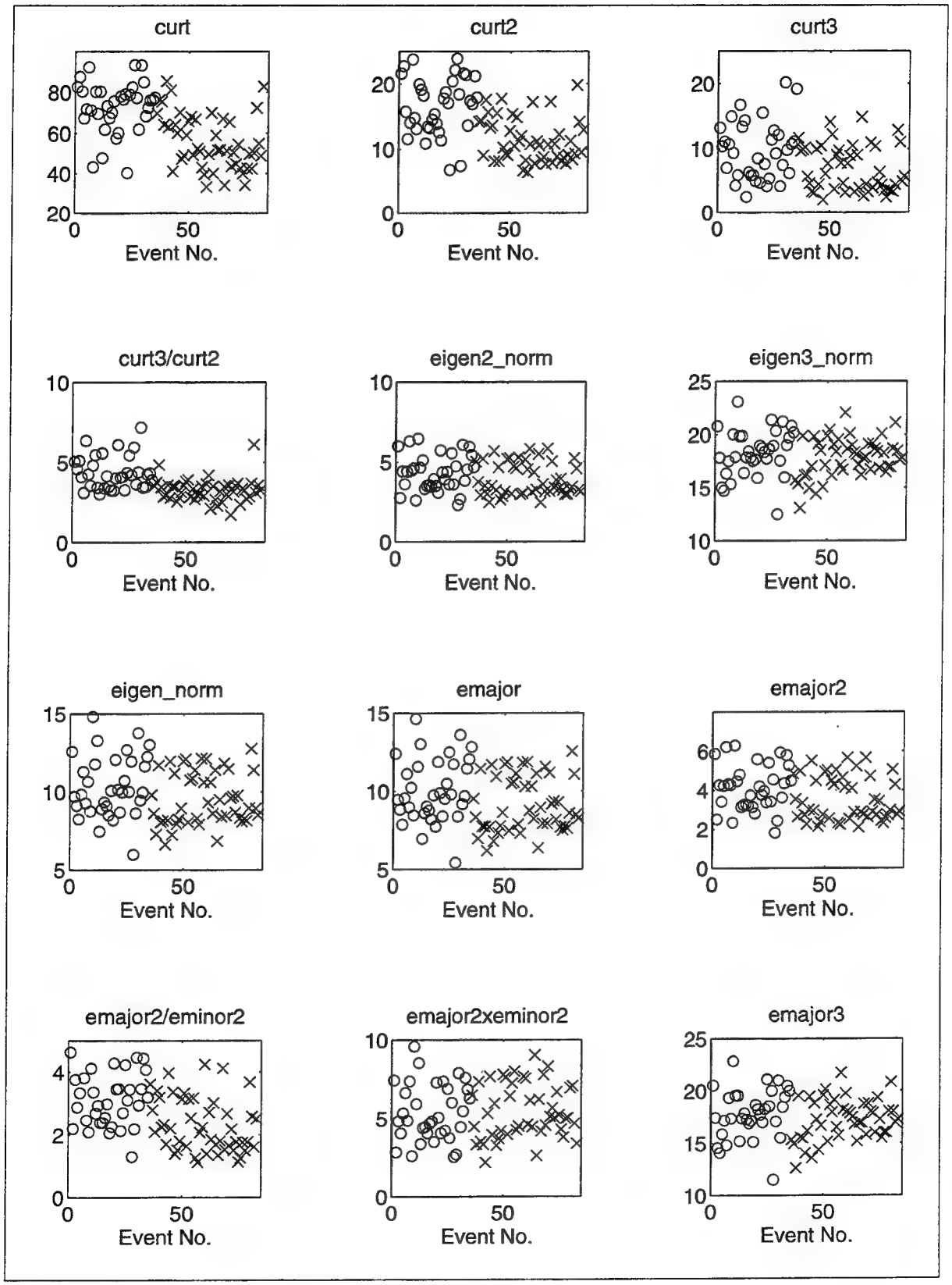

Figure 5. Values of image parameters 1-12 for the NORESS dataset, equalization number 2.

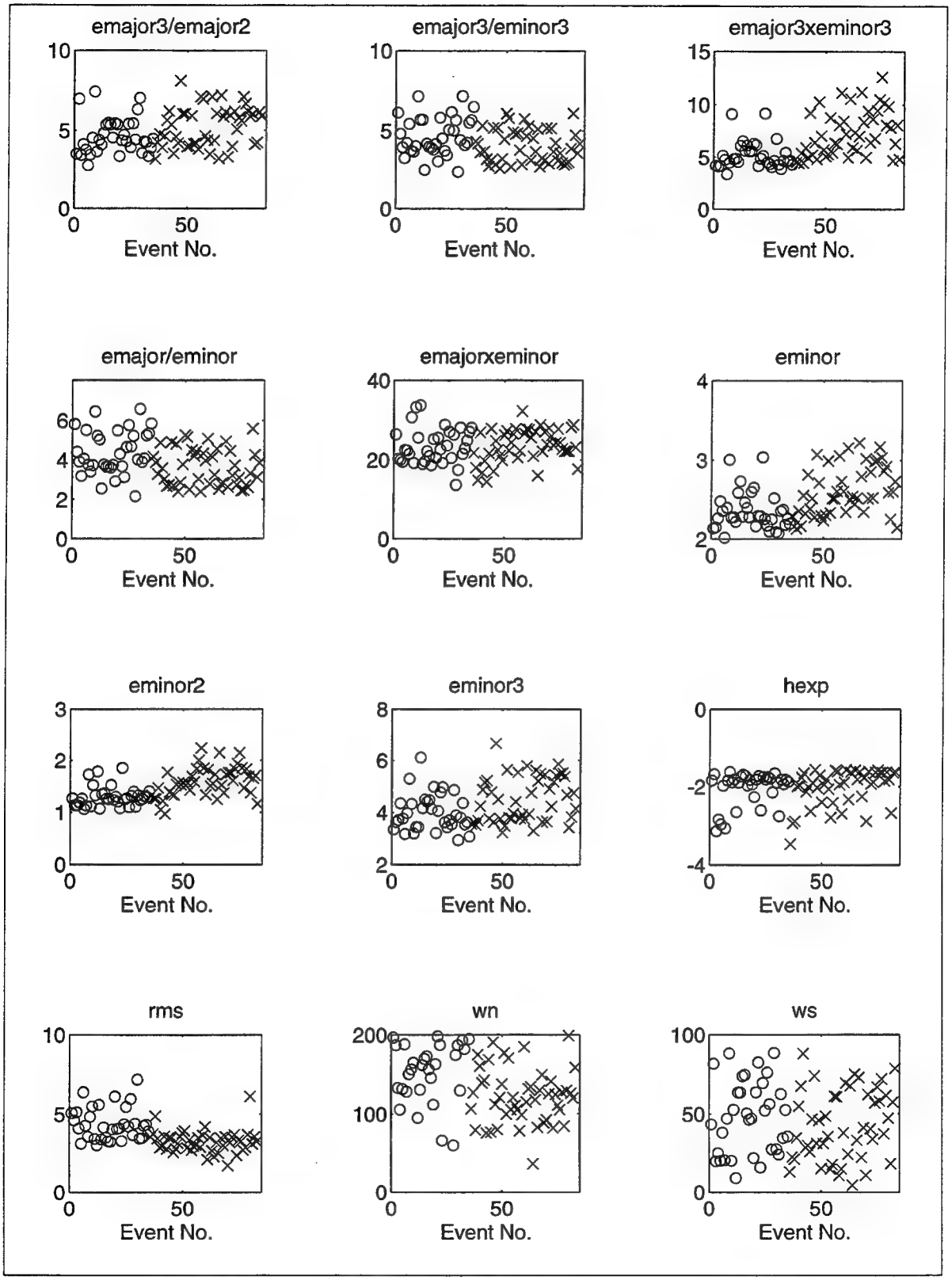

Figure 6. Values of image parameters 13-24 for the NORESS dataset, equalization number 2.

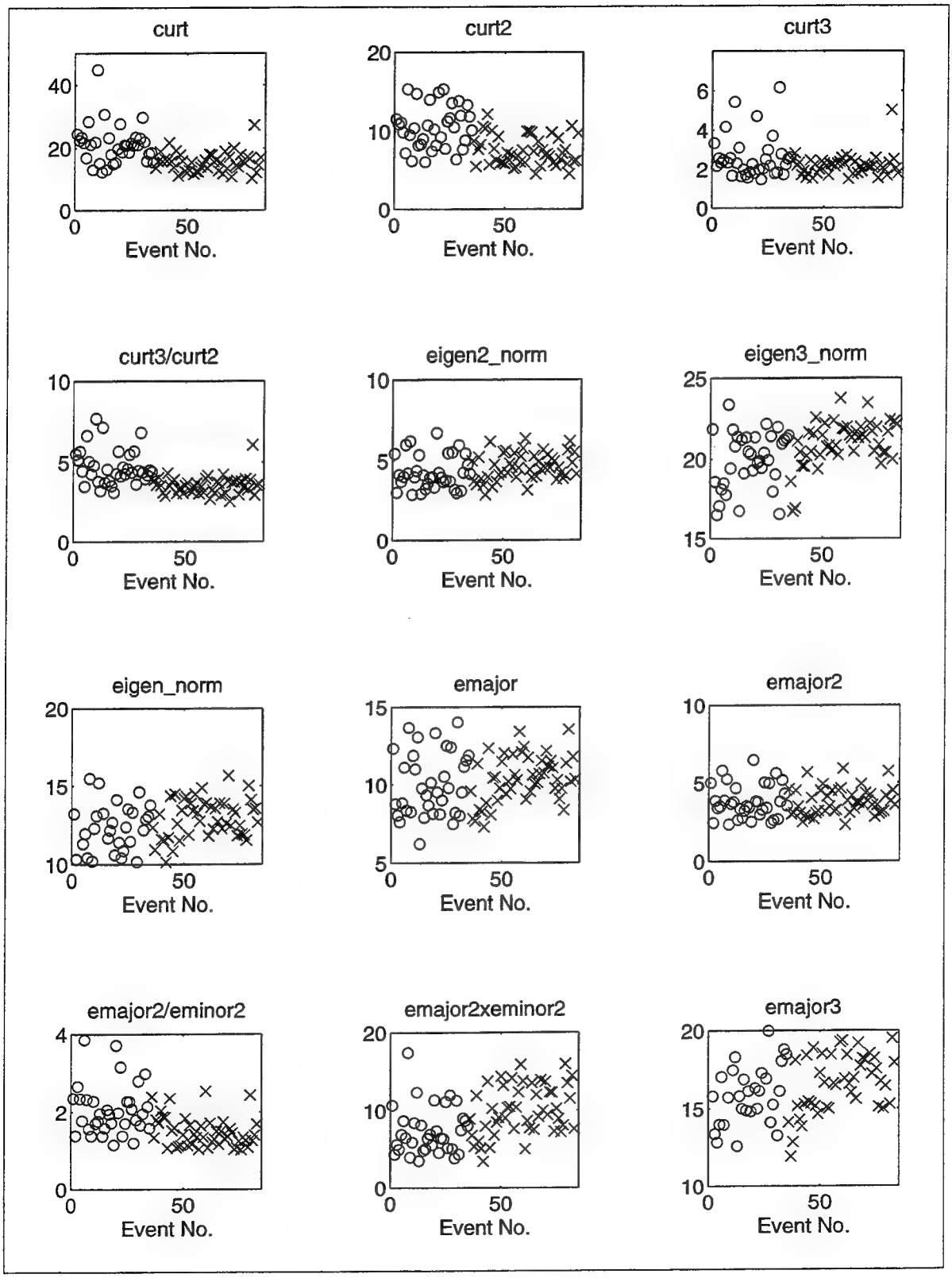

Figure 7. Values of image parameters 1-12 for the NORESS dataset, equalization number 3.

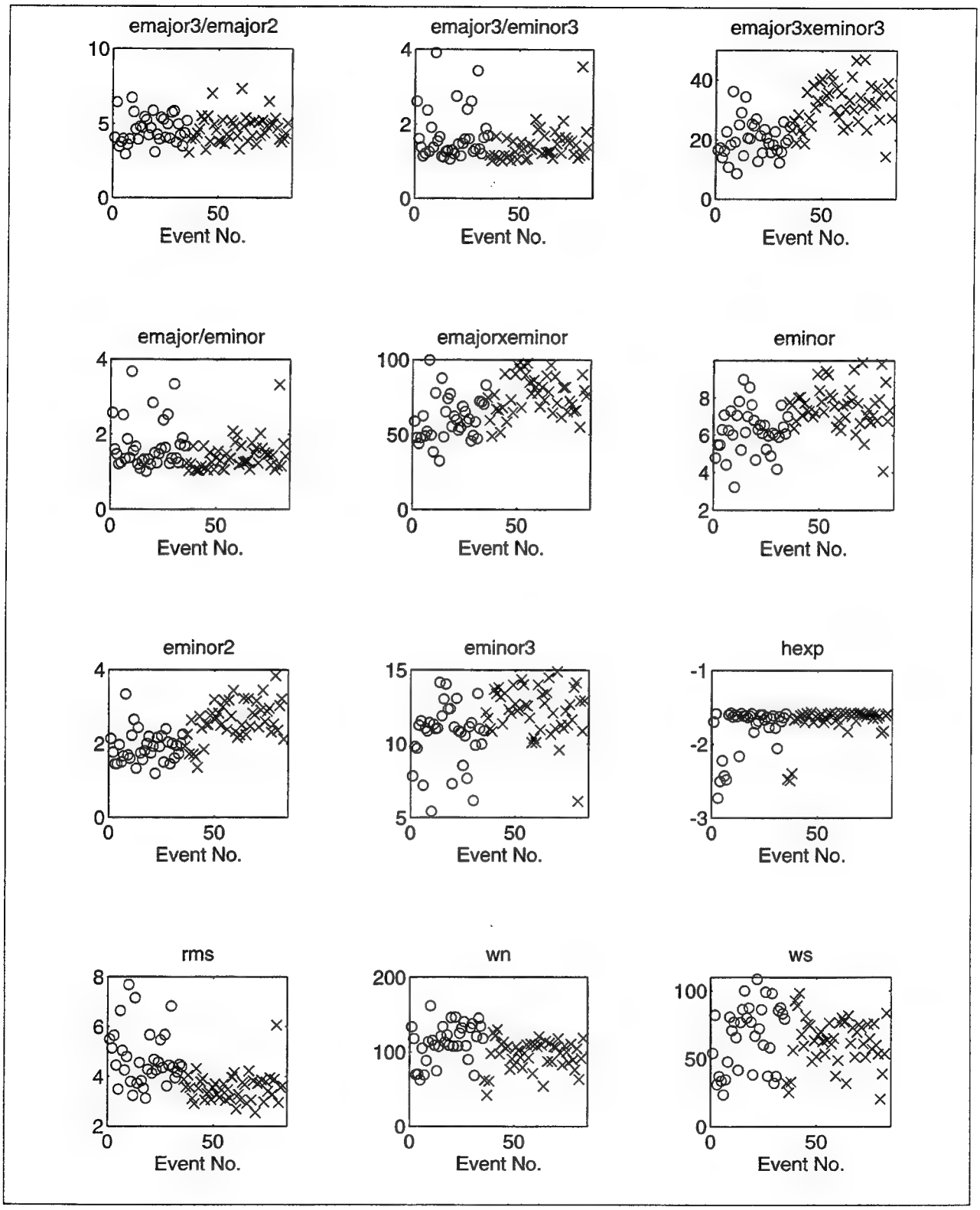

Figure 8. Values of image parameters 13-24 for the NORESS dataset, equalization number 3.

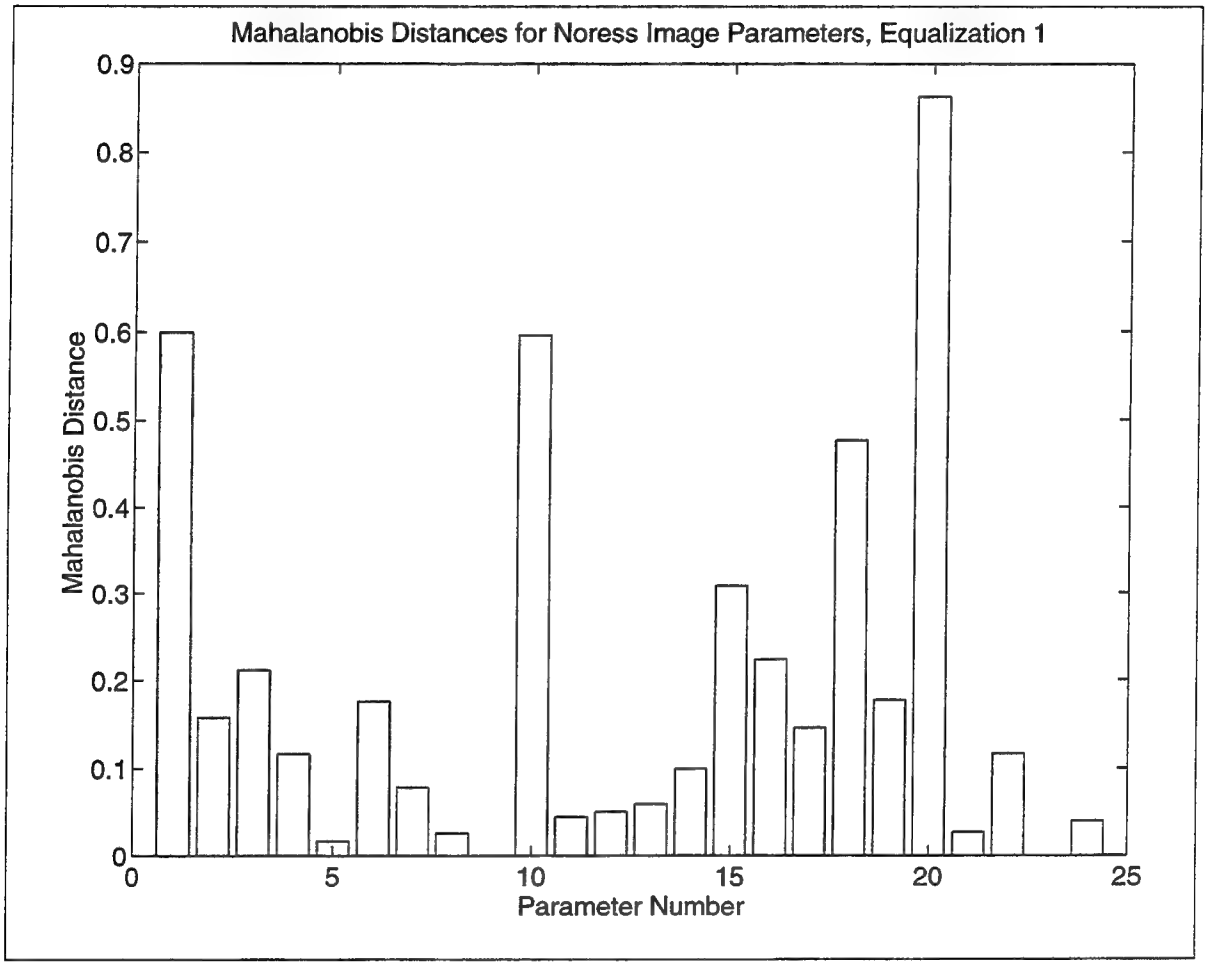

Figure 9. Mahalanobis distances for image parameters for NORESS database, equalization 1.

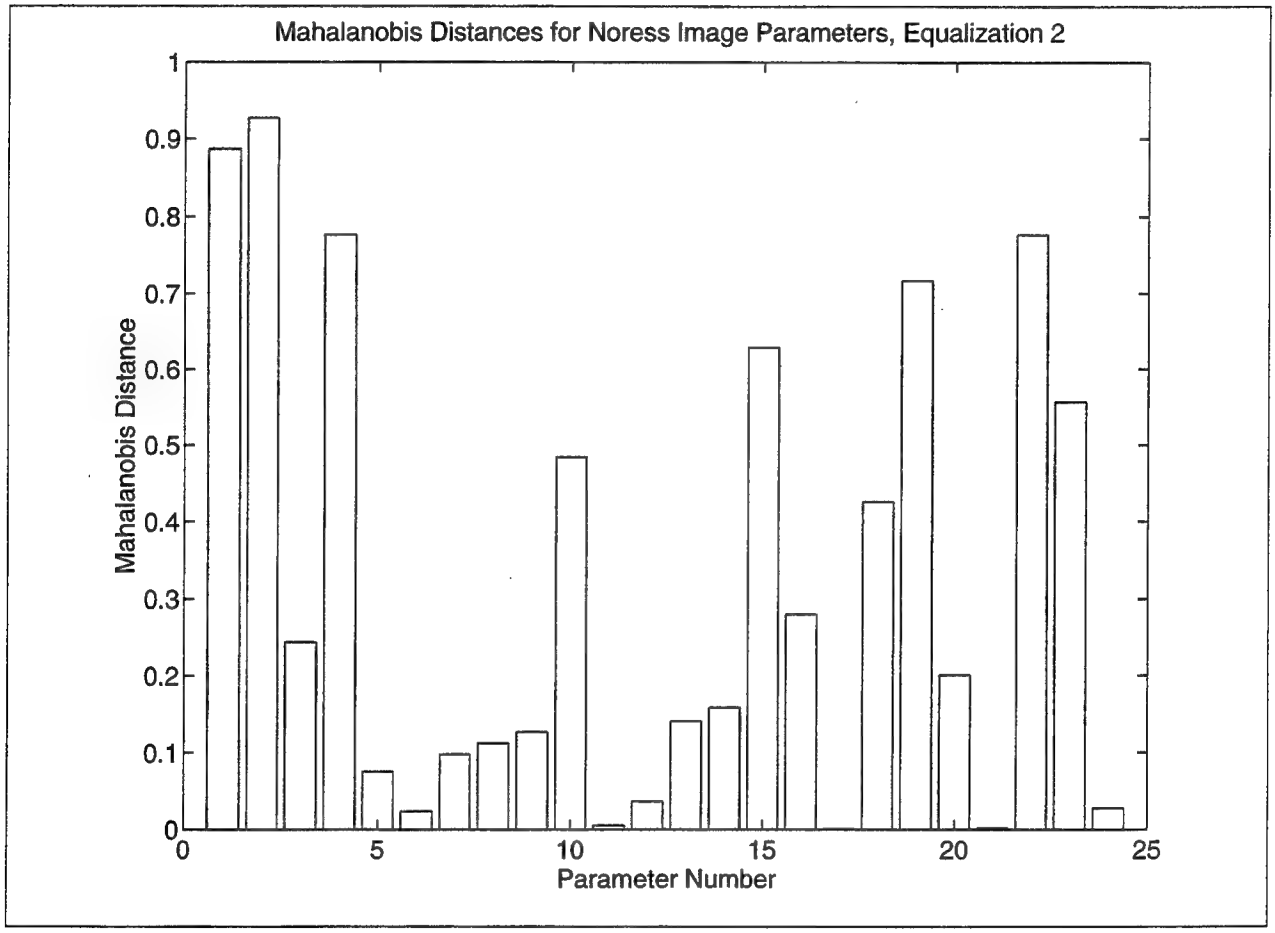

Figure 10. Mahalanobis distances for image parameters for NORESS database, equalization 2.

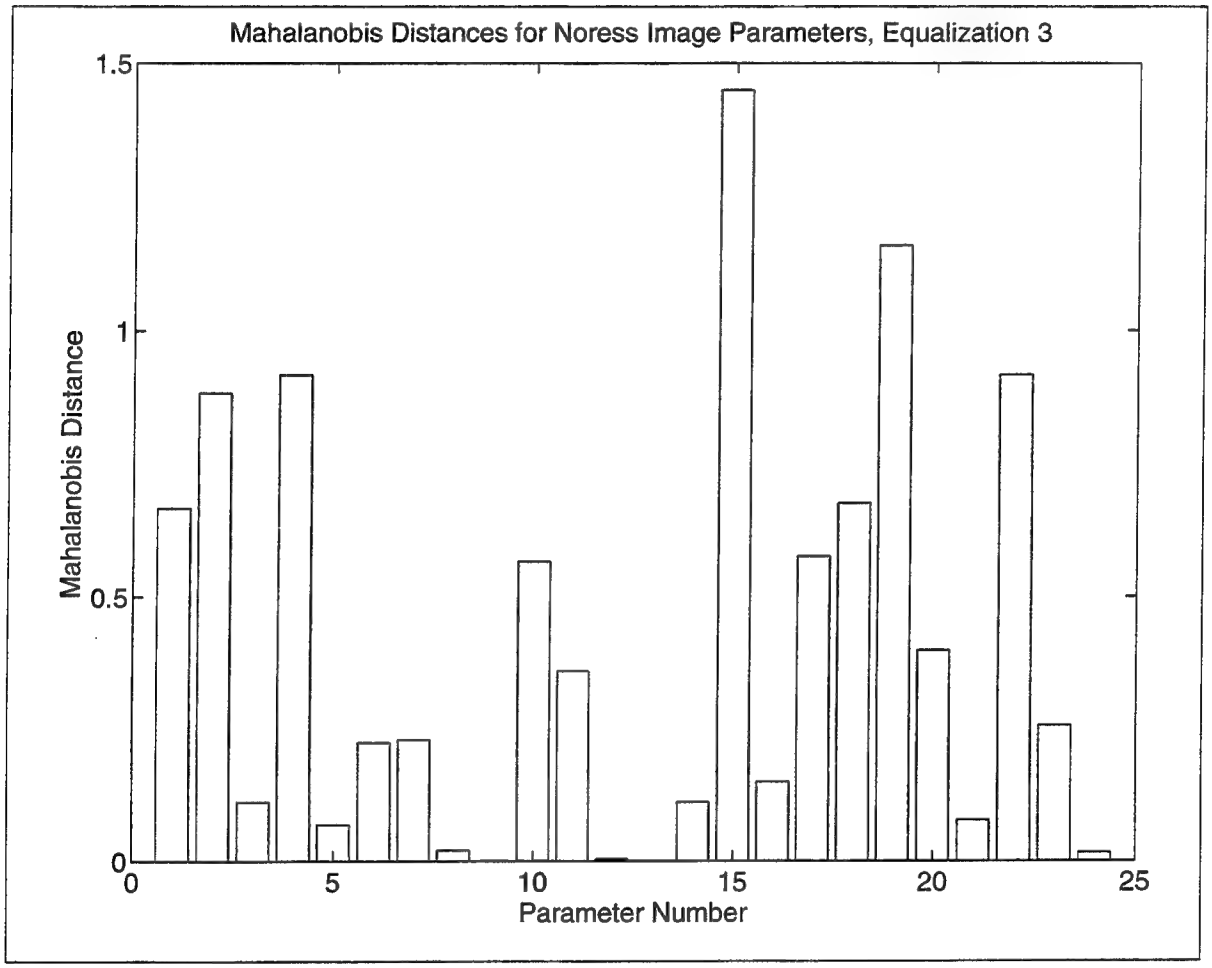

Figure 11. Mahalanobis distances for image parameters for NORESS database, equalization 3.

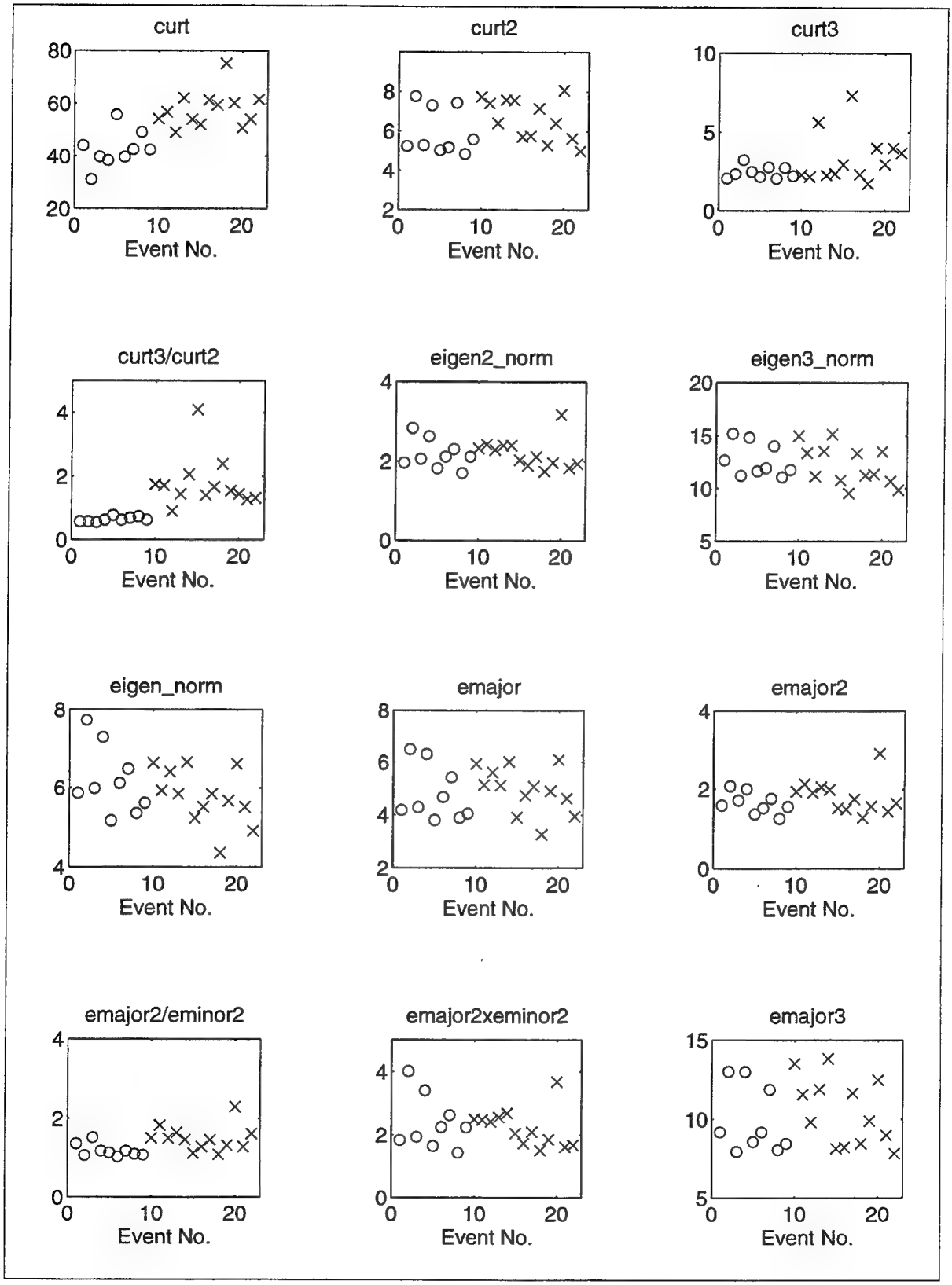

Figure 12. Values of image parameters 1-12 for the Vogtland dataset, equalization number 1.

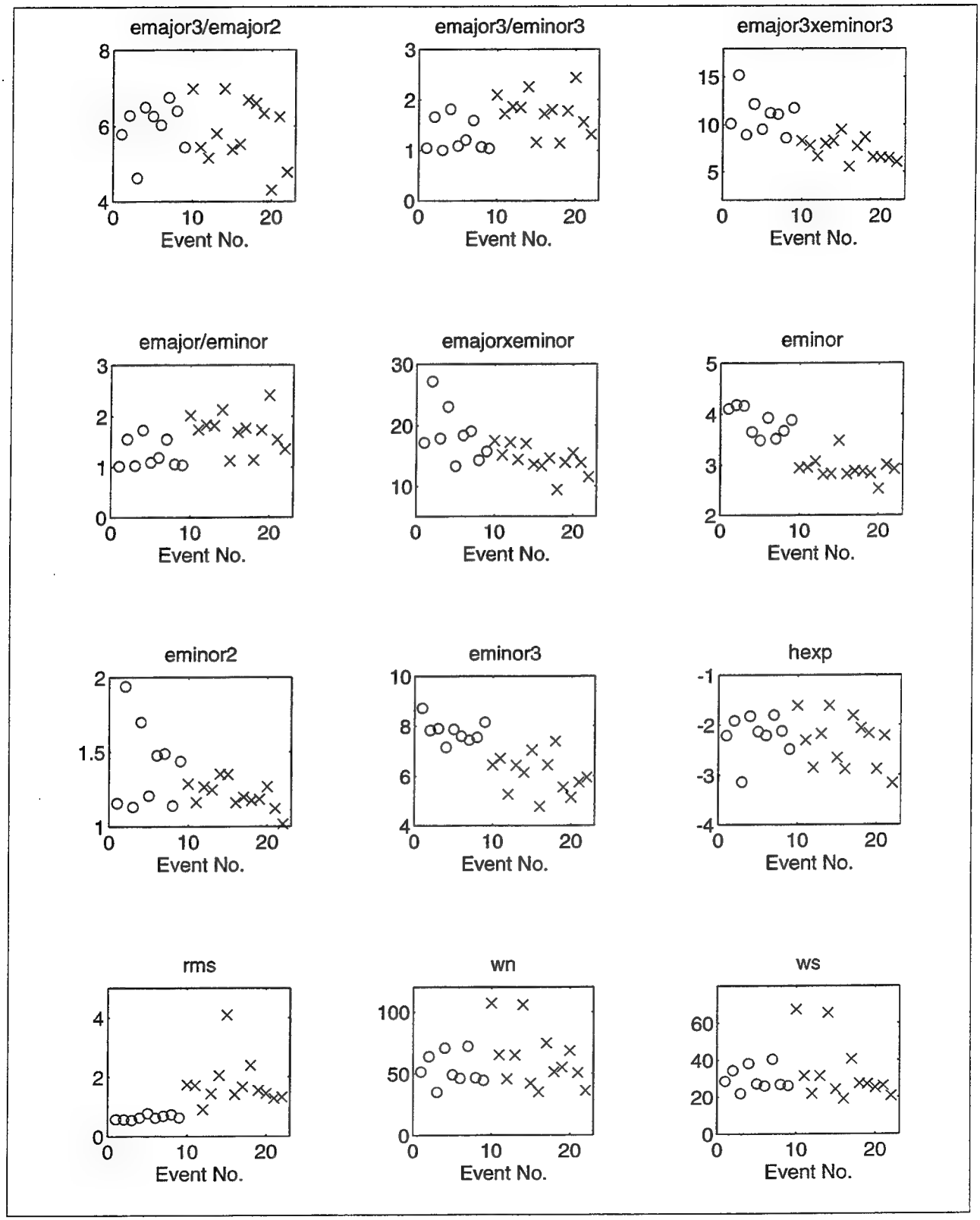

Figure 13. Values of image parameters 13-24 for the Vogtland dataset, equalization number 1.

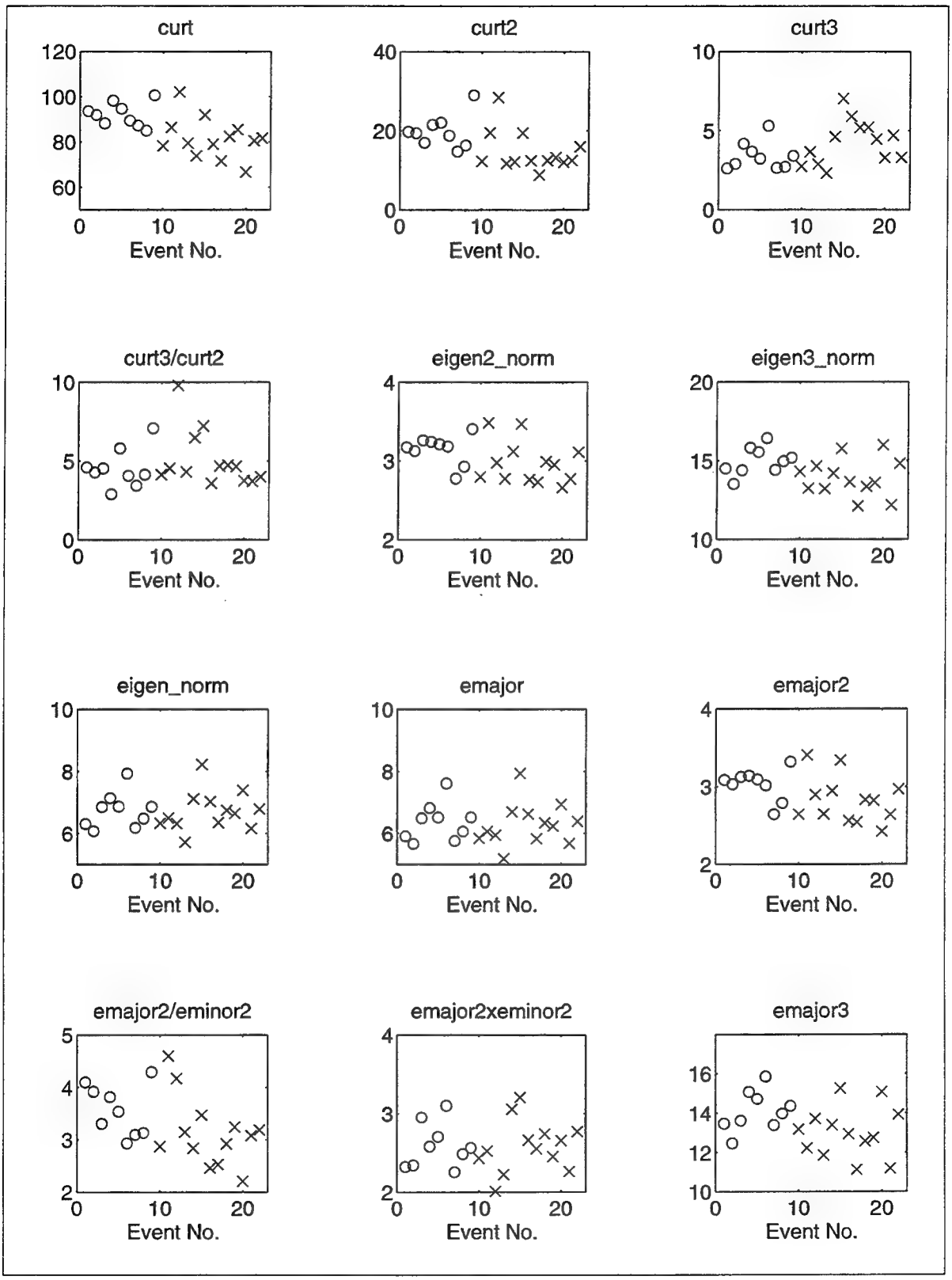

Figure 14. Values of image parameters 1-12 for the Vogtland dataset, equalization number 2.

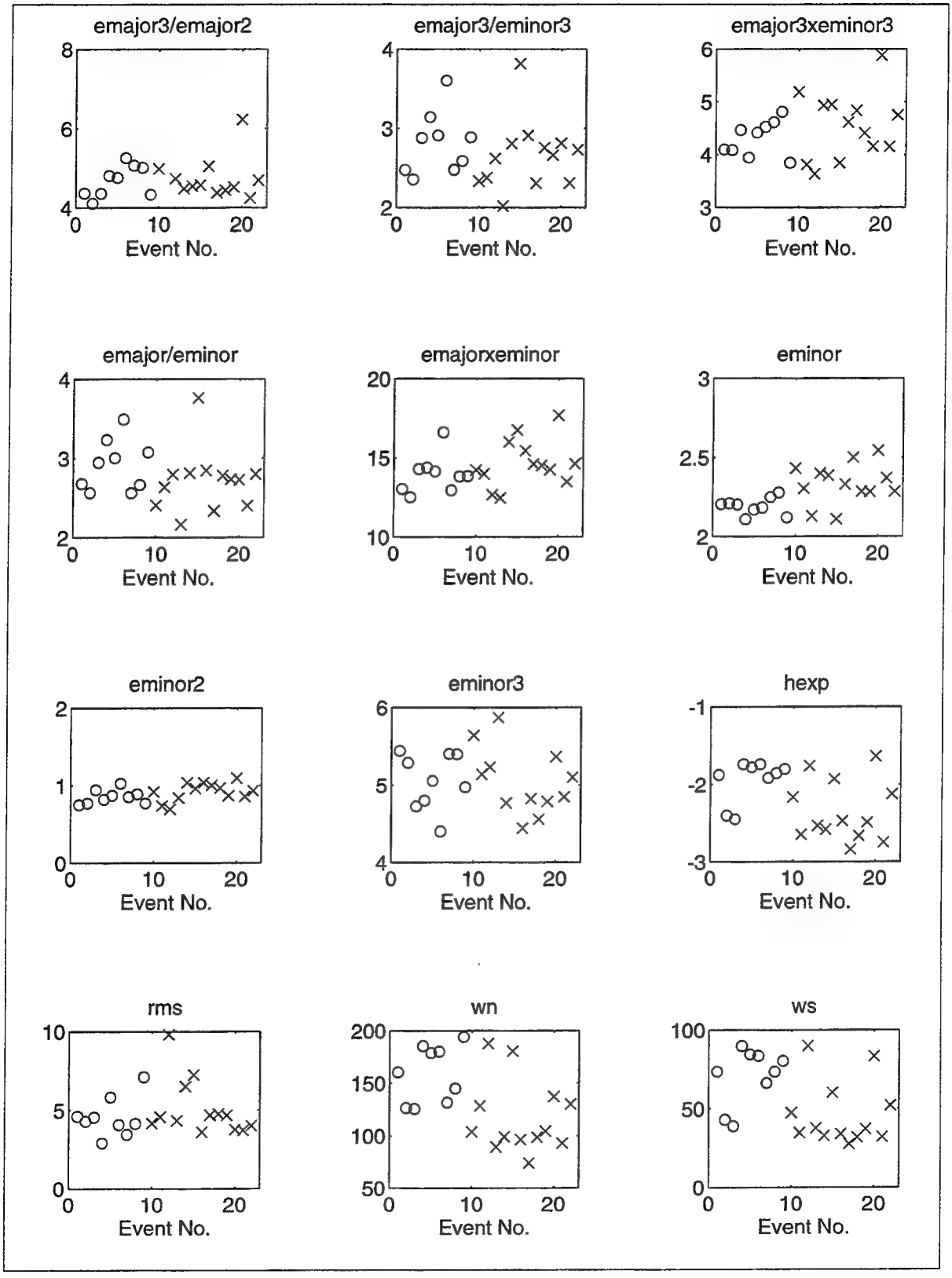

Figure 15. Values of image parameters 13-24 for the Vogtland dataset, equalization number 2.

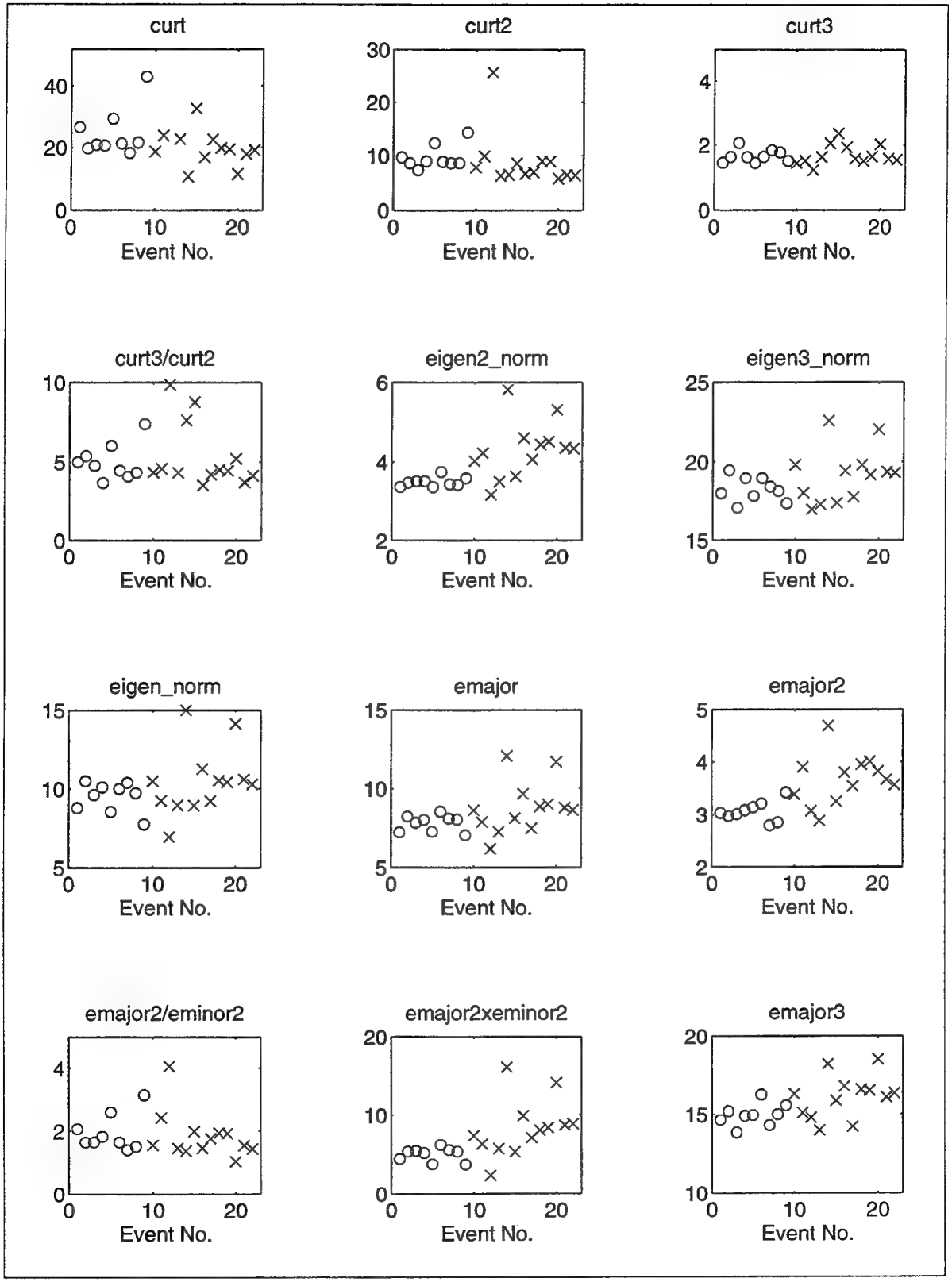

Figure 16. Values of image parameters 1-12 for the Vogtland dataset, equalization number 3.

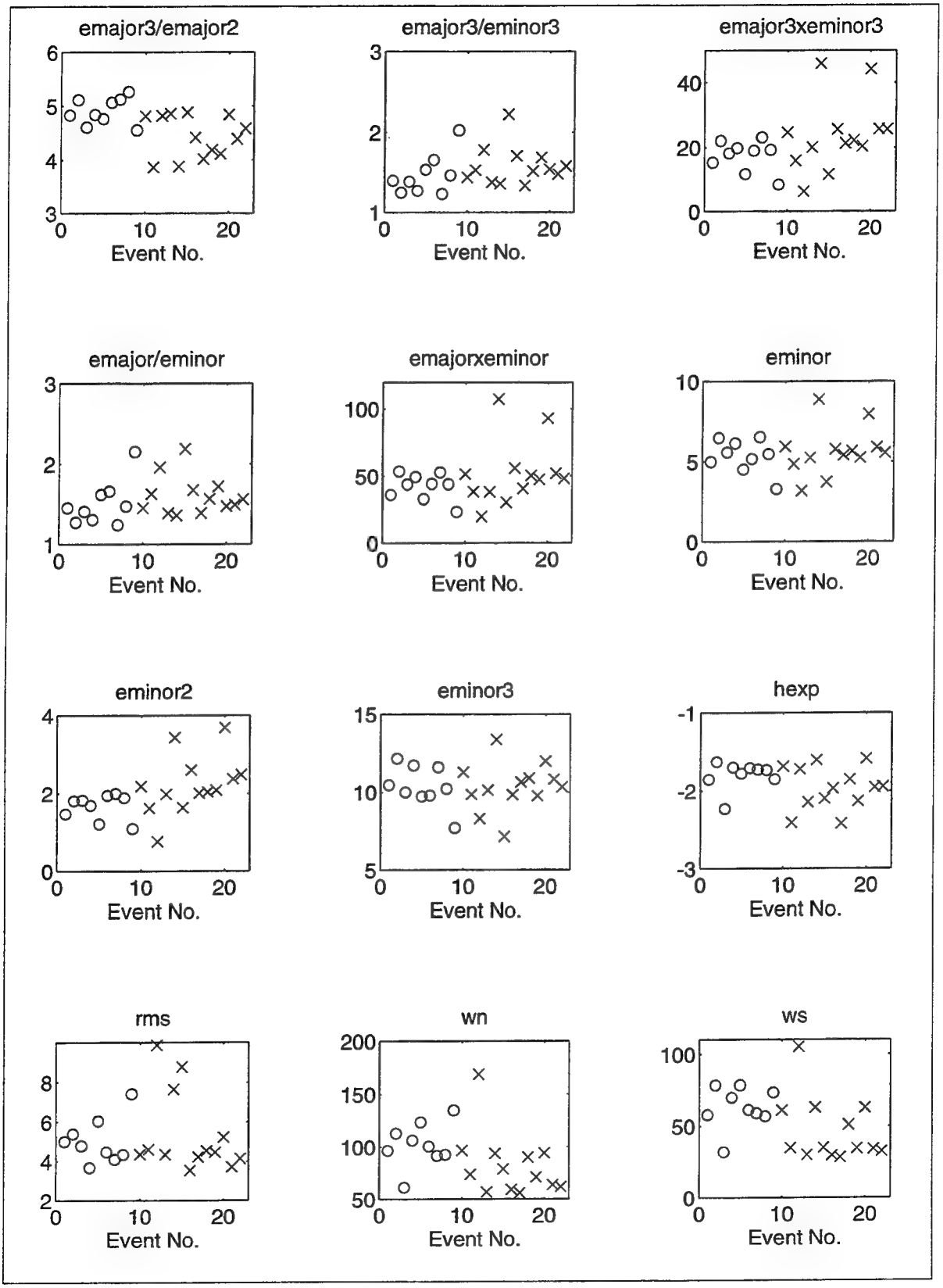

Figure 17. Values of image parameters 13-24 for the Vogtland dataset, equalization number 3.

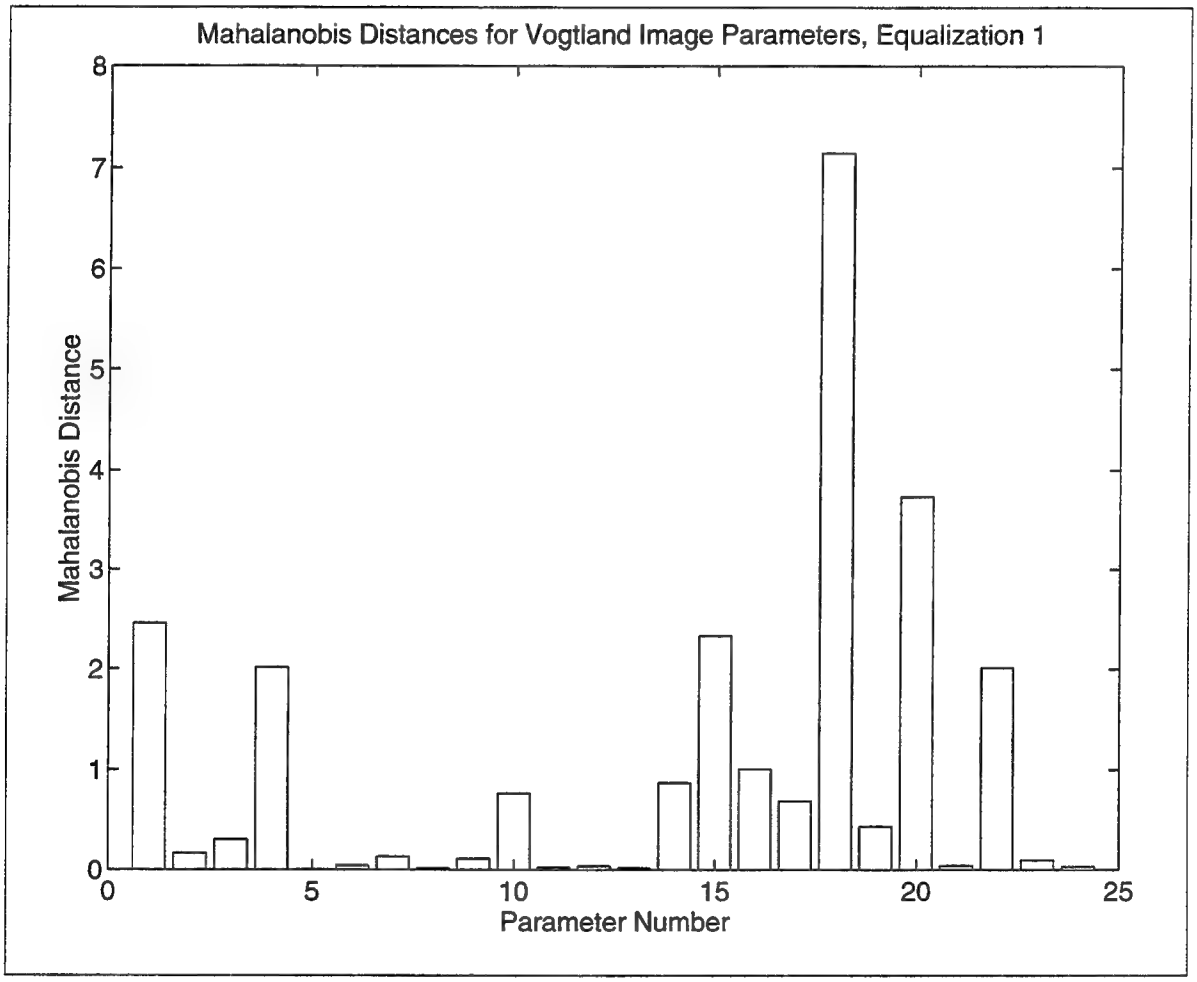

Figure 18. Mahalanobis distances for image parameters for Vogtland database, equalization 1.

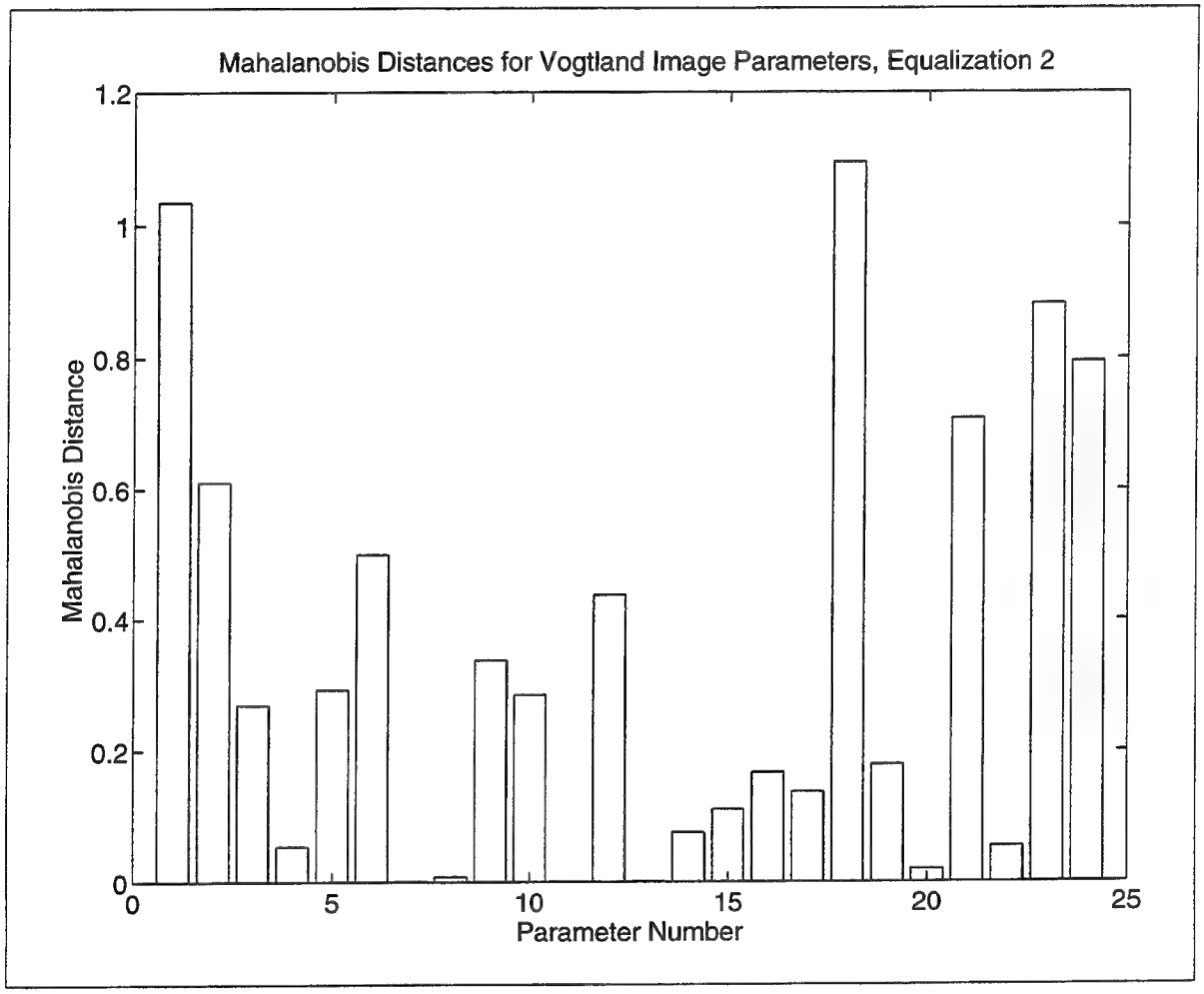

Figure 19. Mahalanobis distances for image parameters for Vogtland database, equalization 2.

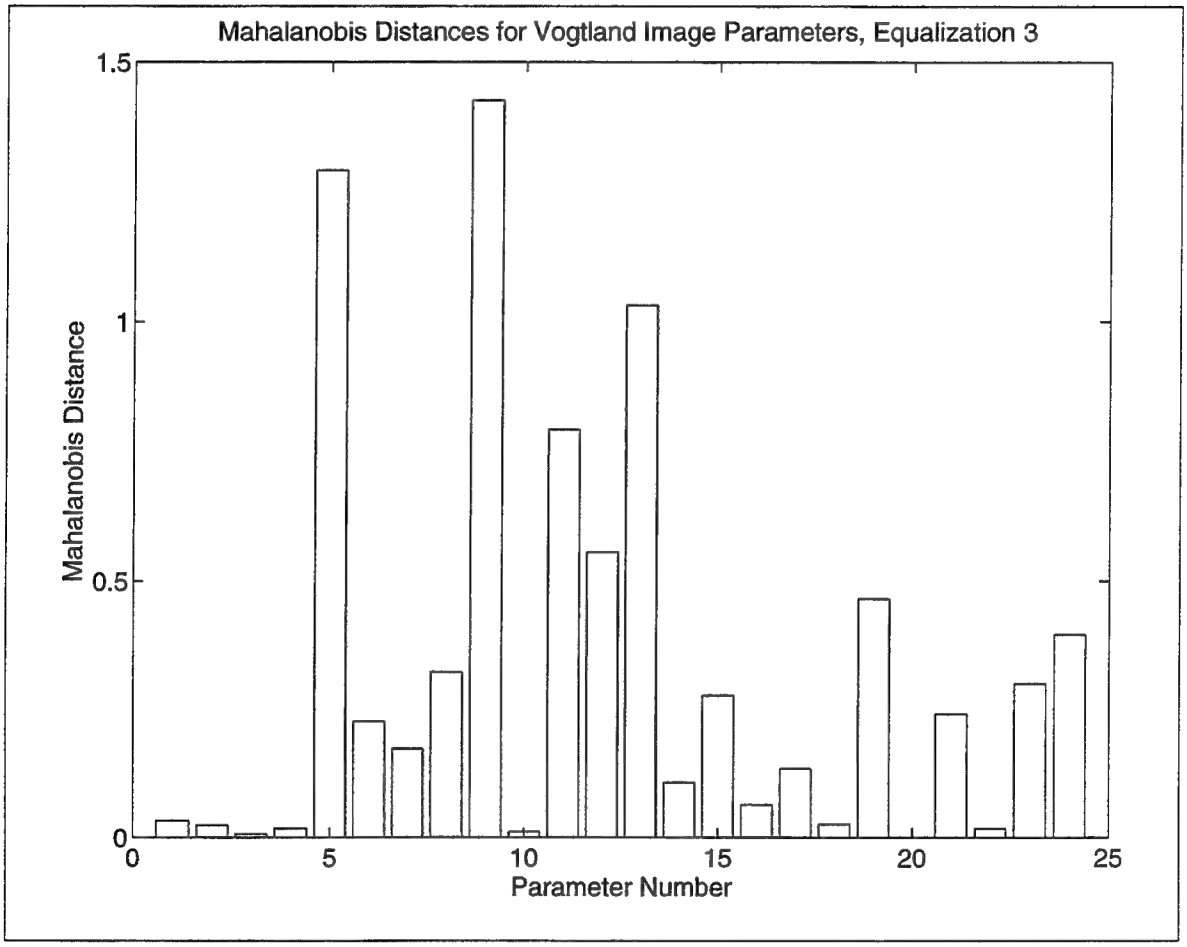

Figure 20. Mahalanobis distances for image parameters for Vogtland database, equalization 3.

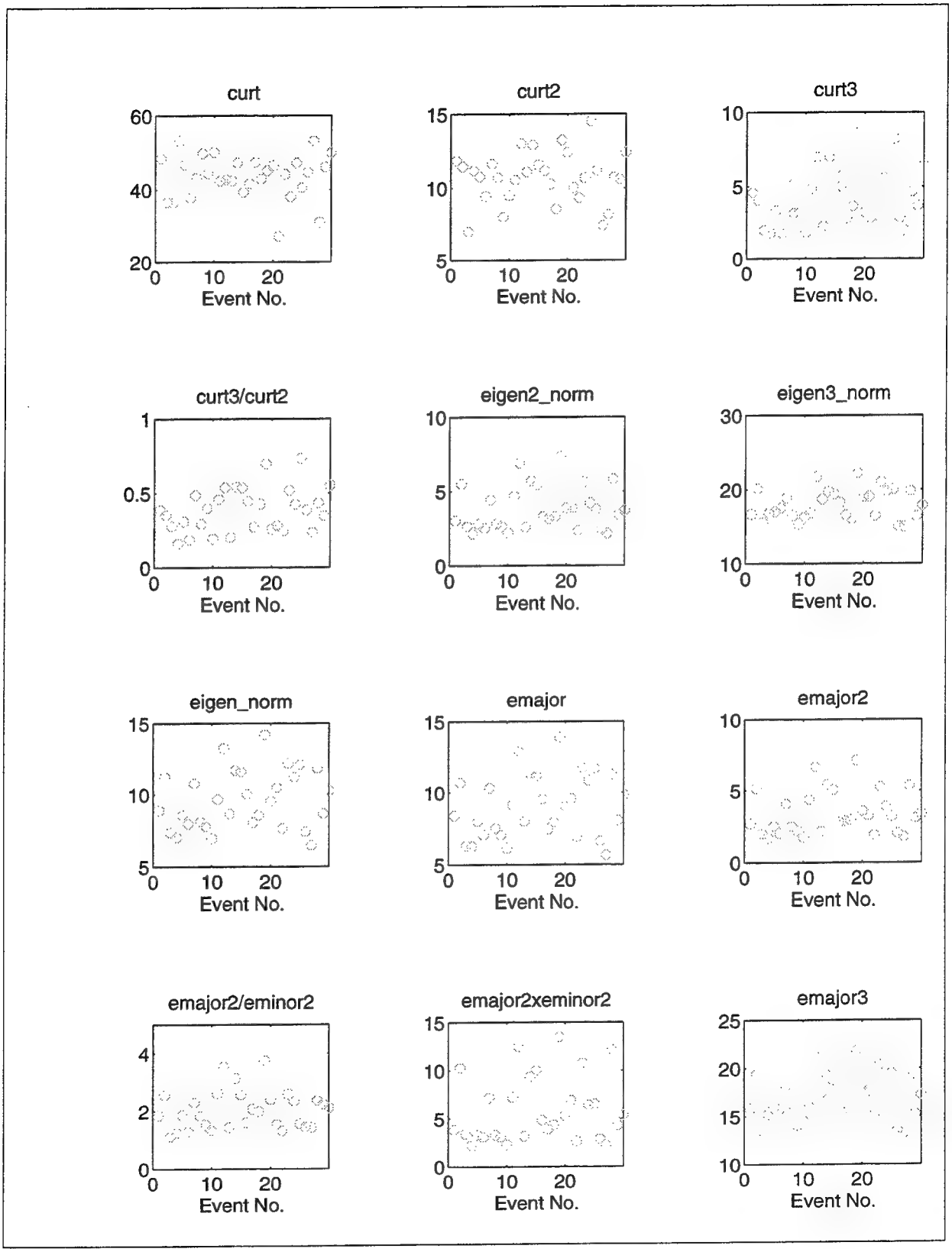

Figure 21. Values of image parameters 1-12 for the Lubin dataset, equalization number 1.

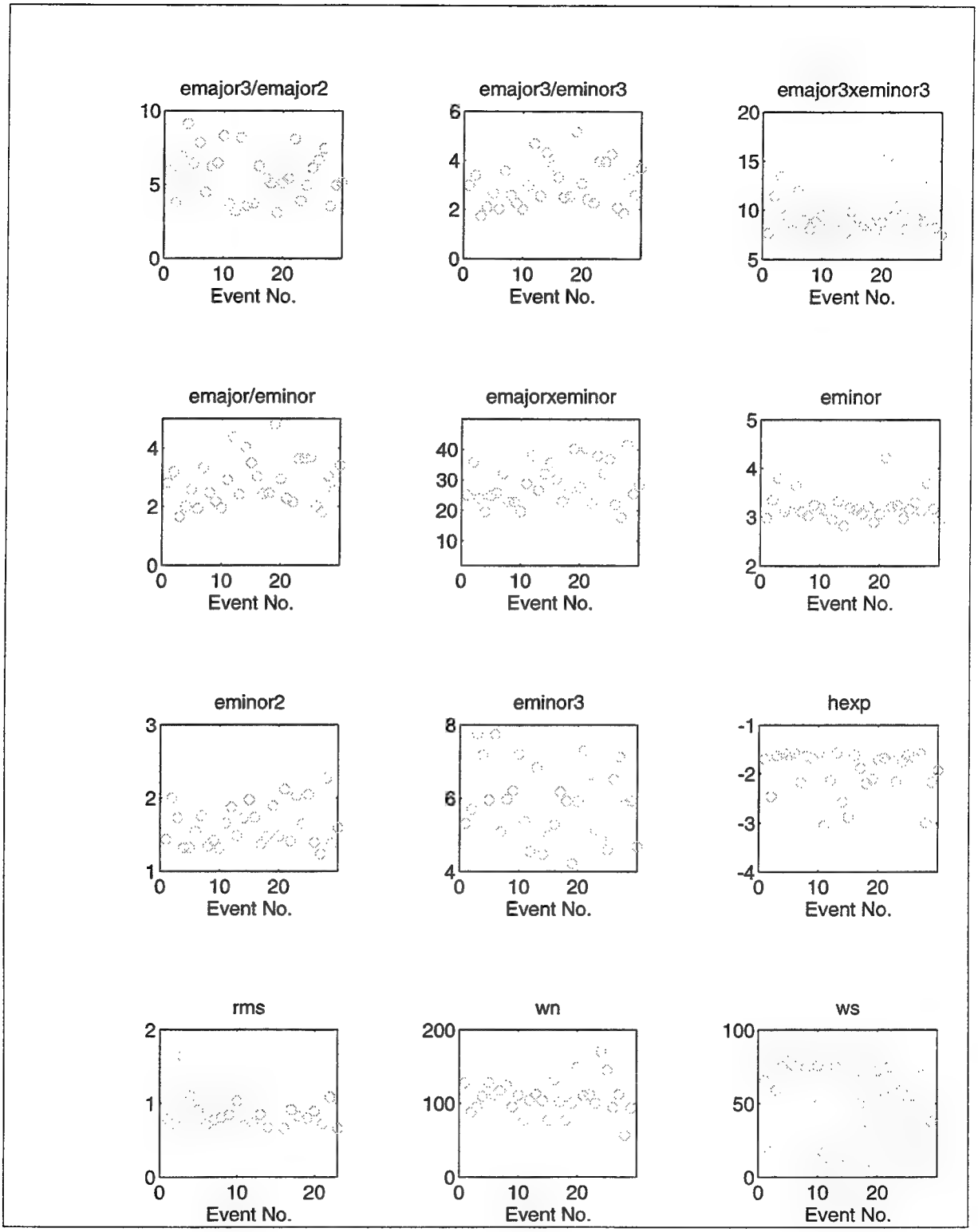

Figure 22. Values of image parameters 12-24 for the Lubin dataset, equalization number 1.

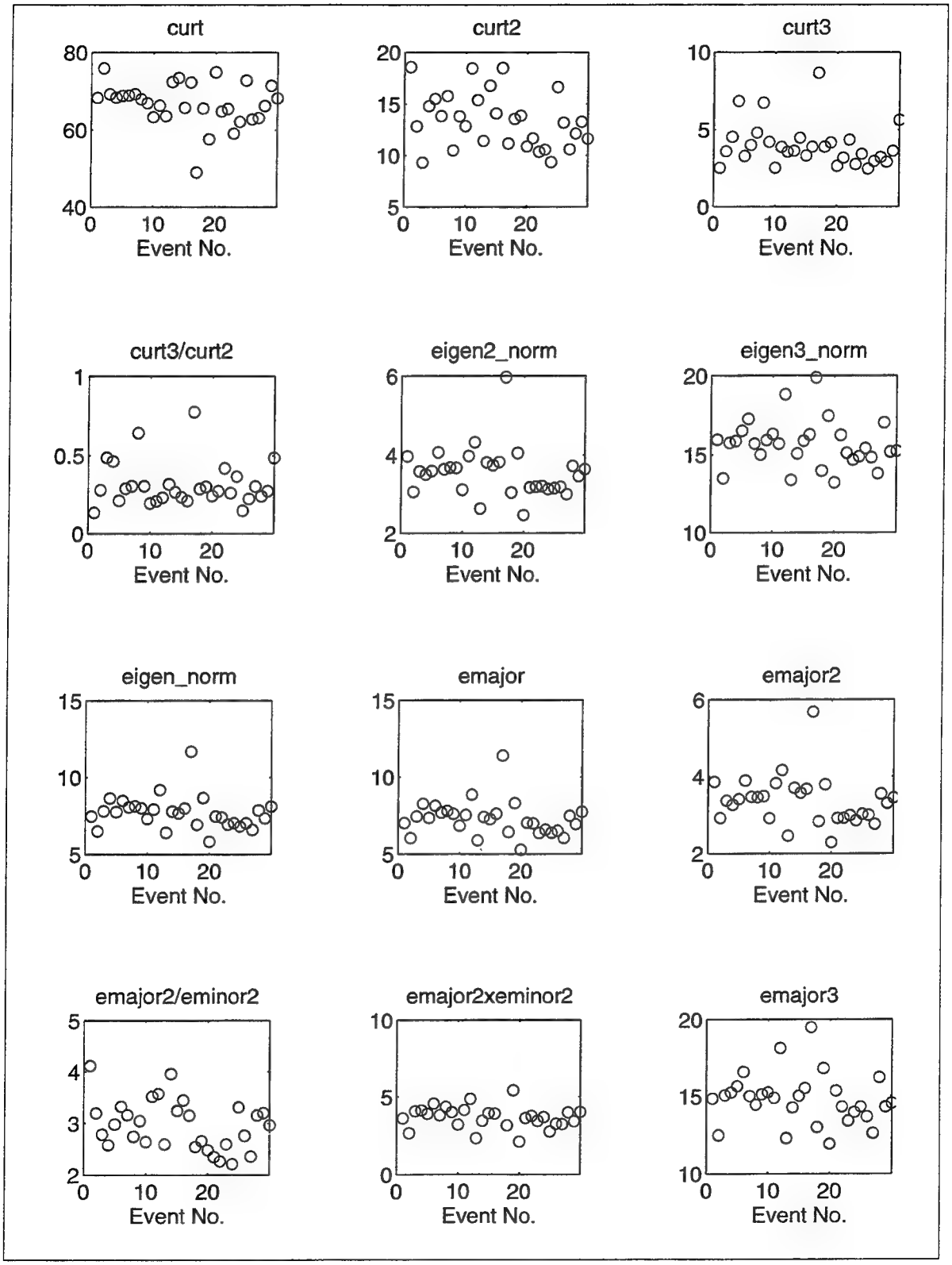

Figure 23. Values of image parameters 1-12 for the Lubin dataset, equalization number 2.

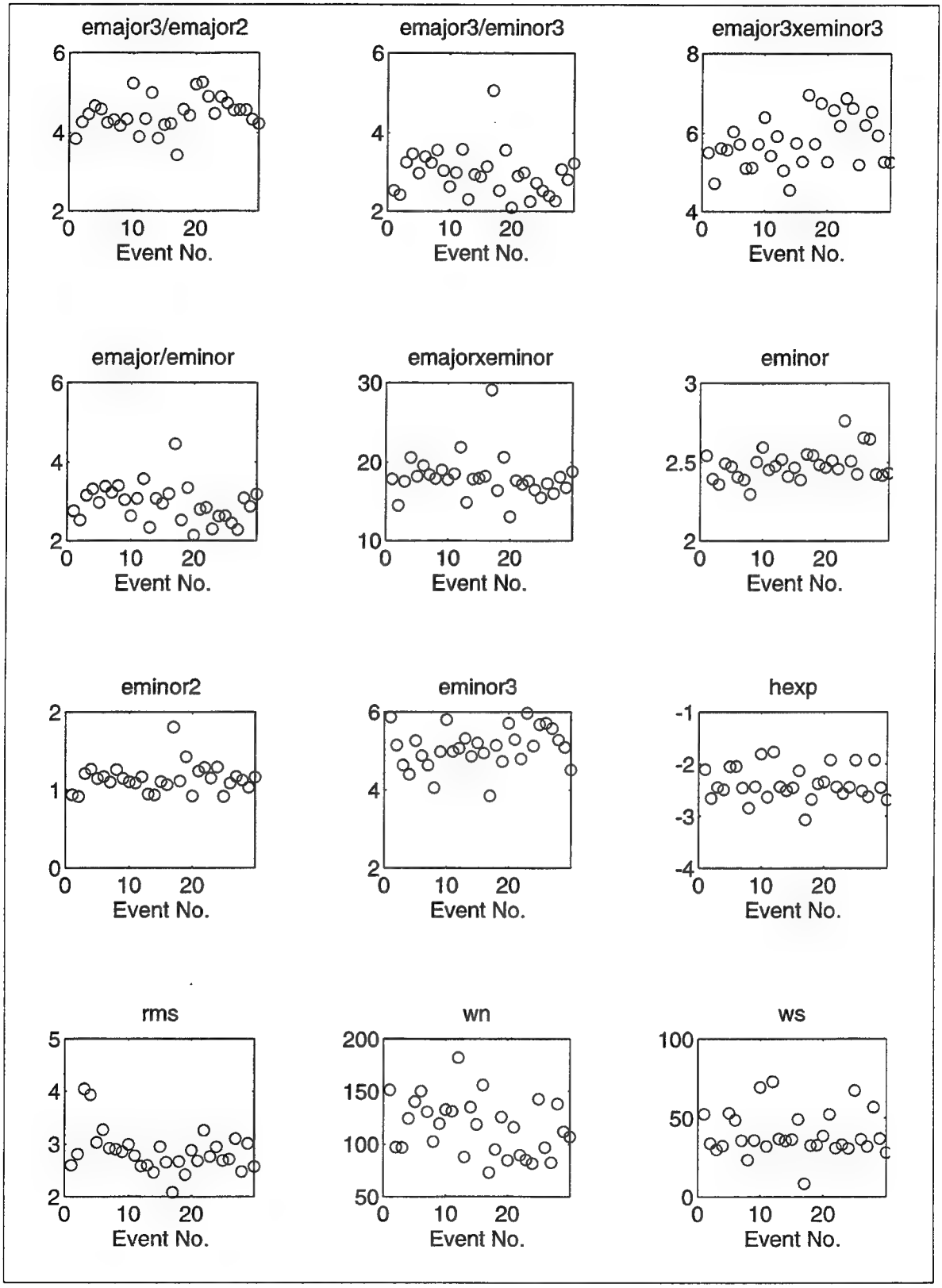

Figure 24. Values of image parameters 12-24 for the Lubin dataset, equalization number 2.

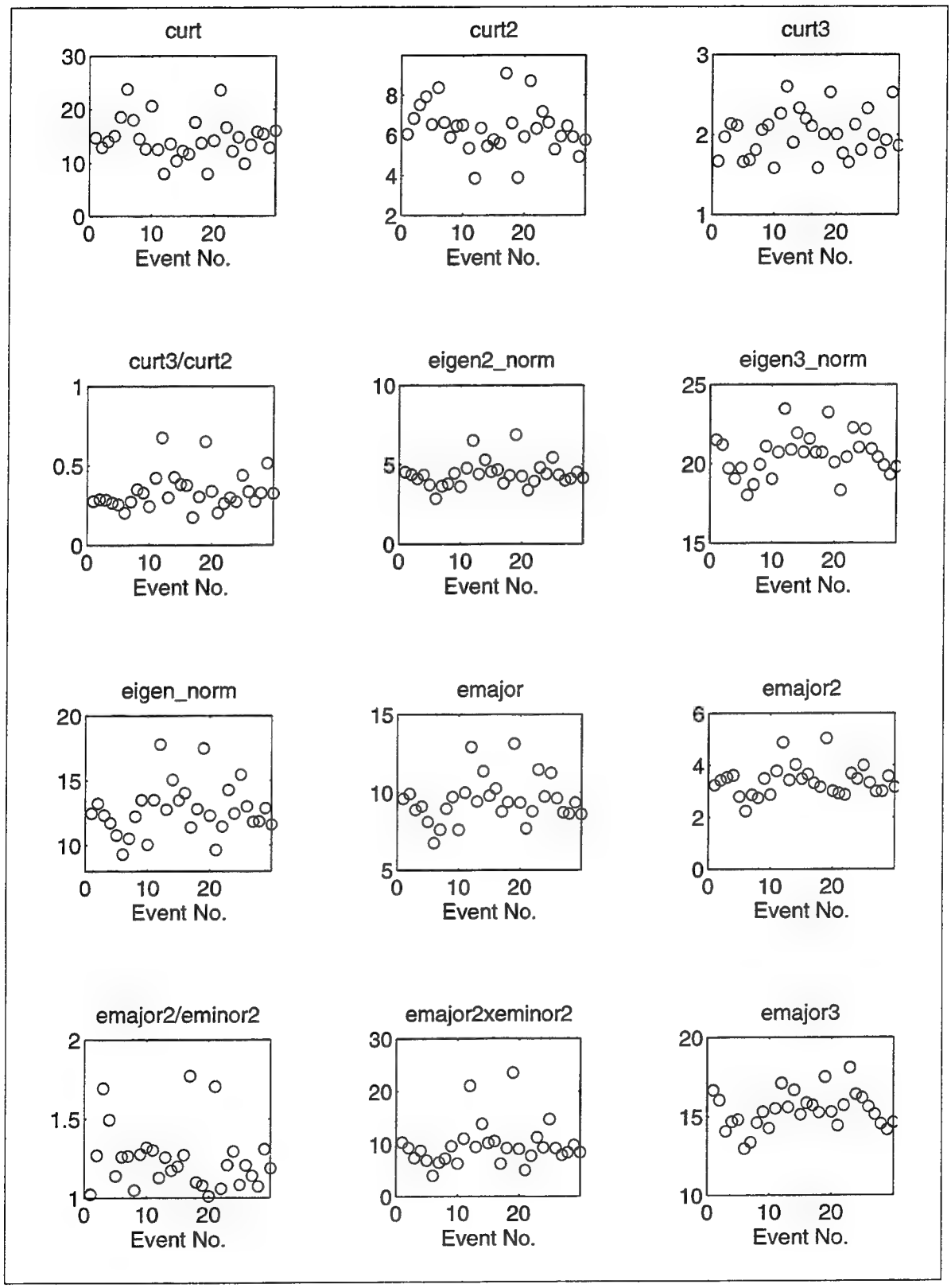

Figure 25. Values of image parameters 1-12 for the Lubin dataset, equalization number 3.

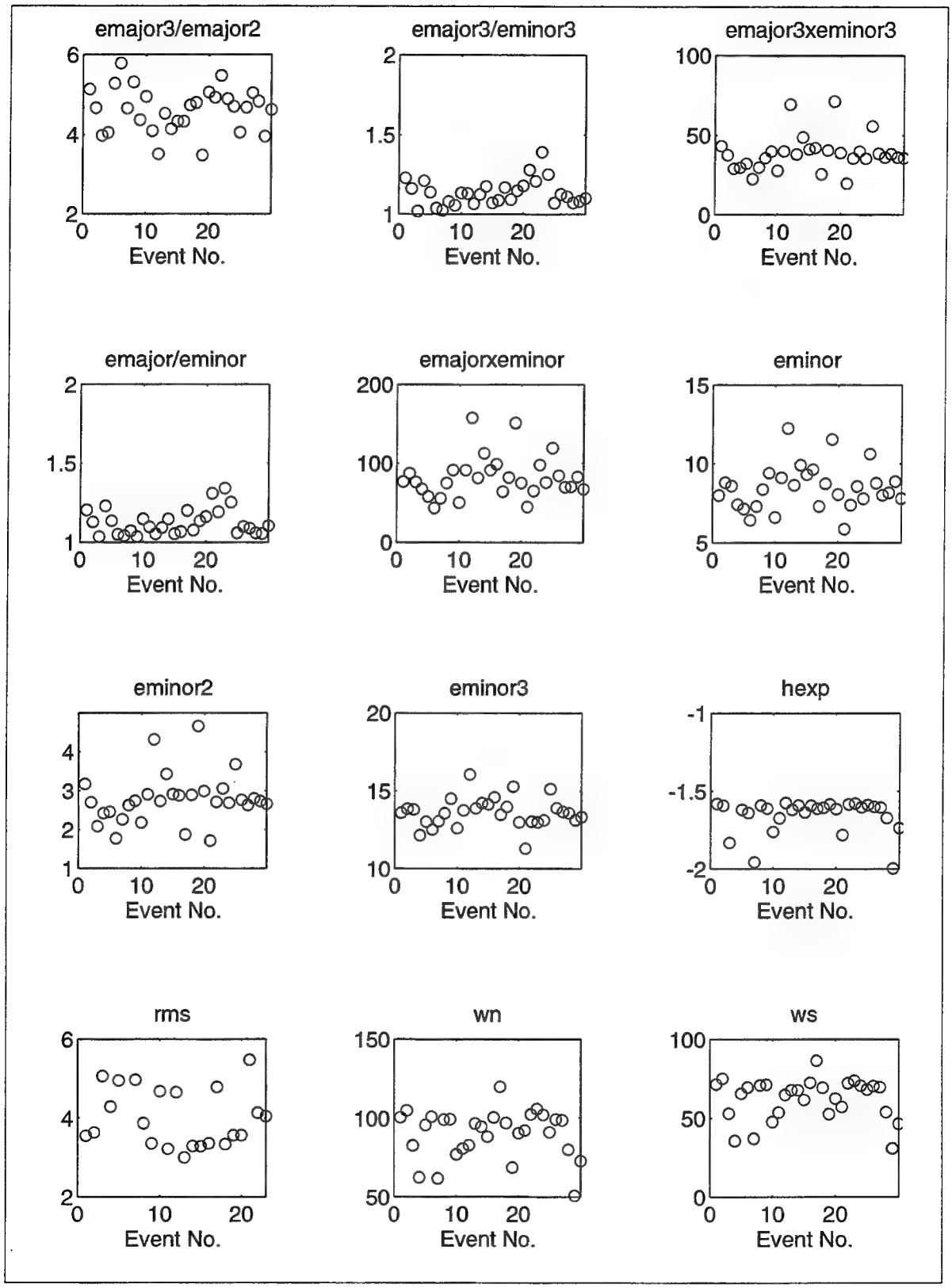

Figure 26. Values of image parameters 12-24 for the Lubin dataset, equalization number 3.

4. Summary and Conclusions

The goal of this research was to determine if parameters extracted from the time-frequency (TF) representations of regional seismograms could be used to identify seismic source types. To accomplish this, we extracted 24 image parameters from the wavenumber spectra of previously identified seismic events from the NORESS, Vogtland, and Lubin ground-truth databases. A total of 135 events were analyzed.

A number of the image parameters were found to provide excellent source identification capability. For example, the eigenvalues of the images and the image kurtosis were found to be useful for the NORESS and Vogtland datasets. The Lubin events, which are all "mining-induced earthquakes", fall within either the earthquake or explosion classes, which corroborates the results of our 1-dimensional study (Pulli and Dysart, 1994). In general, we find that the image parameters extracted from the wavenumber spectral images provide additional useful information for source identification.

If there is a problem with the methodology, it lies in the physical interpretation of the image parameters. Some parameters, such as the characteristic wavelengths, reflect spectral banding in the TF distributions. However, some useful parameters, such as the image eigenvalues, are not readily related to the source physics. To overcome this difficulty, a model study should be undertaken so that image parameters can be extracted from TF plots of model events with known spectral characteristics.

5. References

Cohen, L. (1989), Time-frequency distributions - a review, *Proc. IEEE, 77*, 941-981.

Goff, J.A. and T.H. Jordan (1989), Stochastic modeling of seafloor morphology; inversion of sea beam data for second-order statistics, *J. Geophys. Res., 93*, 13589-13608.

Grant, L. J. Coyne, and F. Ryall (1993), CSS Ground-Truth Database: Version 1 Handbook, Scientific Report No. C93-05, Center for Seismic Studies

Hedlin, M.A., J.B. Minster, and J.A. Orcutt (1989), The time-frequency characteristics of quarry blasts and calibration explosions recorded in Kazakhstan, USSR, *Geophys. J. Int., 99*, 109-121.

Johnson, R.A. and D.W. Weichern (1992), Applied Multivariate Statistical Analysis, Prentice Hall, N.J.

Pulli, J.J. and P.S. Dysart (1994), Development and Testing of a Methodology for Regional Seismic Event Identification in Eurasia, Phillips Laboratory Report

Smith, A.T. (1989), High-frequency seismic observations and models of chemical explosions: implications for the discrimination of ripple-fired mining blasts, *Bull. Seis. Soc. Amer., 79*, 1089-1110.

Prof. Thomas Ahrens
Seismological Lab, 252-21
Division of Geological & Planetary Sciences
California Institute of Technology
Pasadena, CA 91125

Prof. Keiiti Aki
Center for Earth Sciences
University of Southern California
University Park
Los Angeles, CA 90089-0741

Prof. Shelton Alexander
Geosciences Department
403 Deike Building
The Pennsylvania State University
University Park, PA 16802

Dr. Thomas C. Bache, Jr.
Science Applications Int'l Corp.
10260 Campus Point Drive
San Diego, CA 92121 (2 copies)

Prof. Muawia Barazangi
Cornell University
Institute for the Study of the Continent
3126 SNEE Hall
Ithaca, NY 14853

Dr. Douglas R. Baumgardt
ENSCO, Inc
5400 Port Royal Road
Springfield, VA 22151-2388

Dr. T.J. Bennett
S-CUBED
A Division of Maxwell Laboratories
11800 Sunrise Valley Drive, Suite 1212
Reston, VA 22091

Dr. Robert Blandford
AFTAC/TT, Center for Seismic Studies
1300 North 17th Street
Suite 1450
Arlington, VA 22209-2308

Dr. Steven Bratt
ARPA/NMRO
3701 North Fairfax Drive
Arlington, VA 22203-1714

Dale Breding
U.S. Department of Energy
Recipient, IS-20, GA-033
Office of Arms Control
Washington, DC 20585

Dr. Jerry Carter
Center for Seismic Studies
1300 North 17th Street
Suite 1450
Arlington, VA 22209-2308

Mr Robert Cockerham
Arms Control & Disarmament Agency
320 21st Street North West
Room 5741
Washington, DC 20451,

Dr. Zoltan Der
ENSCO, Inc.
5400 Port Royal Road
Springfield, VA 22151-2388

Dr. Stanley K. Dickinson
AFOSR/NM
110 Duncan Avenue
Suite B115
Bolling AFB, DC

Dr Petr Firbas
Institute of Physics of the Earth
Masaryk University Brno
Jecna 29a
612 46 Brno, Czech Republic

Dr. Mark D. Fisk
Mission Research Corporation
735 State Street
P.O. Drawer 719
Santa Barbara, CA 93102

Dr. Cliff Frolich
Institute of Geophysics
8701 North Mopac
Austin, TX 78759

Dr. Holly Given
IGPP, A-025
Scripps Institute of Oceanography
University of California, San Diego
La Jolla, CA 92093

Dr. Jeffrey W. Given
SAIC
10260 Campus Point Drive
San Diego, CA 92121

Dr. Dale Glover
Defense Intelligence Agency
ATTN: ODT-1B
Washington, DC 20301

Dan N. Hagedon
Pacific Northwest Laboratories
Battelle Boulevard
Richland, WA 99352

Dr. James Hannon
Lawrence Livermore National Laboratory
P.O. Box 808, L-205
Livermore, CA 94550

Dr. Roger Hansen
University of Colorado, JSPC
Campus Box 583
Boulder, CO 80309

Prof. David G. Harkrider
Division of Geological & Planetary Sciences
California Institute of Technology
Pasadena, CA 91125

Prof. Danny Harvey
University of Colorado, JSPC
Campus Box 583
Boulder, CO 80309

Prof. Donald V. Helmberger
Division of Geological & Planetary Sciences
California Institute of Technology
Pasadena, CA 91125

Prof. Eugene Herrin
Geophysical Laboratory
Southern Methodist University
Dallas, TX 75275

Prof. Robert B. Herrmann
Department of Earth & Atmospheric Sciences
St. Louis University
St. Louis, MO 63156

Prof. Lane R. Johnson
Seismographic Station
University of California
Berkeley, CA 94720

Prof. Thomas H. Jordan
Department of Earth, Atmospheric &
Planetary Sciences
Massachusetts Institute of Technology
Cambridge, MA 02139

Robert C. Kemerait
ENSCO, Inc.
445 Pineda Court
Melbourne, FL 32940

U.S. Dept of Energy
Max Koontz, NN-20, GA-033
Office of Research and Develop.
1000 Independence Avenue
Washington, DC 20585

Dr. Richard LaCoss
MIT Lincoln Laboratory, M-200B
P.O. Box 73
Lexington, MA 02173-0073

Prof. Charles A. Langston
Geosciences Department
403 Deike Building
The Pennsylvania State University
University Park, PA 16802

Jim Lawson, Chief Geophysicist
Oklahoma Geological Survey
Oklahoma Geophysical Observatory
P.O. Box 8
Leonard, OK 74043-0008

Prof. Thorne Lay
Institute of Tectonics
Earth Science Board
University of California, Santa Cruz
Santa Cruz, CA 95064

Dr. William Leith
U.S. Geological Survey
Mail Stop 928
Reston, VA 22092

Mr. James F. Lewkowicz
Phillips Laboratory/GPE
29 Randolph Road
Hanscom AFB, MA 01731-3010(2 copies)

Dr. Gary McCartor
Department of Physics
Southern Methodist University
Dallas, TX 75275

Prof. Thomas V. McEvilly
Seismographic Station
University of California
Berkeley, CA 94720

Dr. Keith L. McLaughlin
S-CUBED
A Division of Maxwell Laboratory
P.O. Box 1620
La Jolla, CA 92038-1620

Prof. Bernard Minster
IGPP, A-025
Scripps Institute of Oceanography
University of California, San Diego
La Jolla, CA 92093

Prof. Brian J. Mitchell
Department of Earth & Atmospheric Sciences
St. Louis University
St. Louis, MO 63156

Mr. Jack Murphy
S-CUBED
A Division of Maxwell Laboratory
11800 Sunrise Valley Drive, Suite 1212
Reston, VA 22091 (2 Copies)

Dr. Keith K. Nakanishi
Lawrence Livermore National Laboratory
L-025
P.O. Box 808
Livermore, CA 94550

Prof. John A. Orcutt
IGPP, A-025
Scripps Institute of Oceanography
University of California, San Diego
La Jolla, CA 92093

Dr. Howard Patton
Lawrence Livermore National Laboratory
L-025
P.O. Box 808
Livermore, CA 94550

Dr. Frank Pilotte
HQ AFTAC/TT
1030 South Highway A1A
Patrick AFB, FL 32925-3002

Dr. Jay J. Pulli
Radix Systems, Inc.
201 Perry Parkway
Gaithersburg, MD 20877

Prof. Paul G. Richards
Lamont-Doherty Earth Observatory
of Columbia University
Palisades, NY 10964

Mr. Wilmer Rivers
Multimax Inc.
1441 McCormick Drive
Landover, MD 20785

Dr. Alan S. Ryall, Jr.
Lawrence Livermore National Laboratory
L-025
P.O. Box 808
Livermore, CA 94550

Dr.Chandan K. Saikia
Woodward Clyde- Consultants
566 El Dorado Street
Pasadena, CA 91101

Mr. Dogan Seber
Cornell University
Inst. for the Study of the Continent
3130 SNEE Hall
Ithaca, NY 14853-1504

Secretary of the Air Force
(SAFRD)
Washington, DC 20330

Office of the Secretary of Defense
DDR&E
Washington, DC 20330

Thomas J. Sereno, Jr.
Science Application Int'l Corp.
10260 Campus Point Drive
San Diego, CA 92121

Dr. Michael Shore
Defense Nuclear Agency/SPSS
6801 Telegraph Road
Alexandria, VA 22310

Prof. David G. Simpson
IRIS, Inc.
1616 North Fort Myer Drive
Suite 1050
Arlington, VA 22209

Dr. Jeffrey Stevens
S-CUBED
A Division of Maxwell Laboratory
P.O. Box 1620
La Jolla, CA 92038-1620

Prof. Brian Stump
Los Alamos National Laboratory
EES-3
Mail Stop C-335
Los Alamos, NM 87545

Prof. Tuncay Taymaz
Istanbul Technical University
Dept. of Geophysical Engineering
Mining Faculty
Maslak-80626, Istanbul Turkey

Prof. M. Nafi Toksoz
Earth Resources Lab
Massachusetts Institute of Technology
42 Carleton Street
Cambridge, MA 02142

Dr. Larry Turnbull
CIA-OSWR/NED
Washington, DC 20505

Dr. Karl Veith
EG&G
5211 Auth Road
Suite 240
Suitland, MD 20746

Prof. Terry C. Wallace
Department of Geosciences
Building #77
University of Arizona
Tuscon, AZ 85721

Dr. William Wortman
Mission Research Corporation
8560 Cinderbed Road
Suite 700
Newington, VA 22122

ARPA, OASB/Library
3701 North Fairfax Drive
Arlington, VA 22203-1714

HQ DNA
ATTN: Technical Library
Washington, DC 20305

Defense Technical Information Center
Cameron Station
Alexandria, VA 22314 (2 Copies)

TACTEC
Battelle Memorial Institute
505 King Avenue
Columbus, OH 43201 (Final Report)

Phillips Laboratory
ATTN: GPE
29 Randolph Road
Hanscom AFB, MA 01731-3010

Phillips Laboratory
ATTN: TSML
5 Wright Street
Hanscom AFB, MA 01731-3004

Phillips Laboratory
ATTN: PL/SUL
3550 Aberdeen Ave SE
Kirtland, NM 87117-5776 (2 copies)

Dr. Michel Campillo
Observatoire de Grenoble
I.R.I.G.M.-B.P. 53
38041 Grenoble, FRANCE

Dr. Kin Yip Chun
Geophysics Division
Physics Department
University of Toronto
Ontario, CANADA

Prof. Hans-Peter Harjes
Institute for Geophysic
Ruhr University/Bochum
P.O. Box 102148
4630 Bochum 1, GERMANY

Prof. Eystein Husebye
NTNF/NORSAR
P.O. Box 51
N-2007 Kjeller, NORWAY

David Jepsen
Acting Head, Nuclear Monitoring Section
Bureau of Mineral Resources
Geology and Geophysics
G.P.O. Box 378, Canberra, AUSTRALIA

Ms. Eva Johannisson
Senior Research Officer
FOA
S-172 90 Sundbyberg, SWEDEN

Dr. Peter Marshall
Procurement Executive
Ministry of Defense
Blacknest, Brimpton
Reading FG7-FRS, UNITED KINGDOM

Dr. Bernard Massinon, Dr. Pierre Mechler
Societe Radiomana
27 rue Claude Bernard
75005 Paris, FRANCE (2 Copies)

Dr. Svein Mykkeltveit
NTNT/NORSAR
P.O. Box 51
N-2007 Kjeller, NORWAY (3 Copies)

Dr. Jorg Schlittenhardt
Federal Institute for Geosciences & Nat'l Res.
Postfach 510153
D-30631 Hannover , GERMANY

Dr. Johannes Schweitzer
Institute of Geophysics
Ruhr University/Bochum
P.O. Box 1102148
4360 Bochum 1, GERMANY

Trust & Verify
VERTIC
Carrara House
20 Embankment Place
London WC2N 6NN, ENGLAND